DYNAMICS OF UNDERCUTTERS

BY

KAYODE CARROLL ONI

B.Sc. (Agr.), Ahmadu Sello University, Zaria, Nigeria, 1971
B.S.*, M.S. (Agr. Engg.), Kansas State University, 1974

A DISSERTATION

submitted in partial fulfillment of the

requirements for the degree

DOCTOR OF PHILOSOPHY

College of Engineering

KANSAS STATE UNIVERSITY
Manhattan, Kansas
1981

ACKNOWLEDGEMENT

The author is highly indebted to the Federal Government of Nigeria and Ahmadu Bello University, Zaria, Nigeria for the sponsorship offered him to pursue this program of study.

The author wishes to acknowledge, with thanks, the contributions of his Major Professor, Dr. W.H. Johnson, toward this study. His academic guidance and assistance throughout the course of this study were highly instrumental to the attainment of the author's goal.

The author also wishes to express gratitude to his co-major Professor, Dr. S.J. Clark, whose consistent guidance and encouragement made this study possible. His understanding and counseling during this investigation are fondly remembered with gratitude.

The author expresses a depth of gratitude to Dr. G.A. Milliken for serving on his committee and for the countless hours of guidance during the statistical analysis of this study. Special appreciation is extended to Dr. D.S. Chung for serving on the author's committee and for his valuable suggestions. The author also wishes to thank Dr. E.C. Lindly for serving on his committee and for his academic support.

The author expresses deep gratitude to Dr. M.L. Hayden for the use of Civil Engineering Soil Testing Laboratory and for his many valuable suggestions and assistance.

Sincere gratitude and appreciation are extended to Mrs. Wy Johnson whose moral and material support for the author and his family made the completion of this study possible.

A depth of gratitude is extended to Mr. Darryl Oard for his involvement in the fabrication and installation of the facilities used for this investigation.

The author wishes to express profound gratitude to his wife, Lois, for standing by him and for her understanding at critical times during the conduct of this research.

Finally, the author is deeply grateful for the support and understanding of his mother, Mrs. Lydia Oni.

TABLE OF CONTENTS

	Page
Acknowledgement	ii
List of Tables	vii
List of Figures	viii
List of Frequently Used Symbols	ix
CHAPTER I	
Introduction	1
CHAPTER II	
Review of Literature	5
2.1 Engineering Properties of Agricultural Soils	5
2.2 The Use of Artificial Soils in Tillage Research	9
2.3 Mechanics of Soil Cutting	10
2.4 Tillage Sweep Design	12
2.5 Application of Similitude Techniques to Tillage Research	16
CHAPTER III	
Design Equations for Undercutter Blades	18
CHAPTER IV	
Mathematical Model	22
4.1 Forces on the Tool	23
4.2 Forces on the Soil Segment	23
4.3 Draft Force	26
CHAPTER V	
Equipment Design	28
CHAPTER VI	
Experimental Procedure	33
6.1 Soil Preparation	33
6.2 Soil Strength Properties	33

Page

6.3 Experimental Design 39

6.4 Data Acquisition and Reduction 41

CHAPTER VII

Results and Discussions 48

7.1 Experimental Study 48

7.2 Analytical Study 49

7.3 Statistical Analysis of the Data 52

7.4 Discussion of Results 56

7.4.1 Influence of Soil Depth on Draft 56

7.4.2 Influence of Tool Velocity on Draft 63

7.4.3 Influence of Nose Angle on Draft 63

7.4.4 Influence of Slide Angle on Draft 63

7.4.5 Influence of Lift Height on Draft 66

7.5 Optimum Combination of Factors 66

7.6 Model Selection 73

CHAPTER VIII

Summary and Conclusions 76

8.1 Summary 76

8.2 Conclusions 77

8.3 Suggestions for Future Work 77

References 79

APPENDICES

Appendix A.4 Force Analysis on an Undercutter 85

Appendix A.4.1 Geometric Elements of a Soil Segment 90

Appendix B.6.1 Soil Density Data for Varying Soil Depth 92

Appendix B.6.2 Computer Program for Designing Undercutter Blades 93

		Page
Appendix C.7.1	Observed and Predicted Results	94
Appendix C.7.2	Computer Program for the Analytical Result Using Minicomputer	97
Appendix C.7.3	Computer Printout for the Analytical (Math) Model Using Minicomputer	99
Appendix C.7.4	Generated Draft and Pdraft Data for Varying Soil Depth	101
Appendix C.7.5	Generated Draft and Pdraft Data for Varying Slide Angle	107

LIST OF TABLES

Table		Page
6.1	Result of Periodic Soil Property Tests	35
6.2	The Central Composite Statistical Design for the Investigation	35
6.3	Geometric Elements for Designing Model Tools	42
7.1	Backward Elimination Procedure for Experimental Model- Draft	53
7.2	Backward Elimination Procedure for Analytical Model-Pdraft	54
7.3	Experimental Model (Draft) and Analytical Model (Pdraft) Data for Different Soil Depths	57
7.4	Experimental Model (Draft) and Analytical Model (Pdraft) for Different Tool Slide Angle	59
7.5	Influence of Tool Slide Angle on Draft and Pdraft for Varying Levels of Velocity	68
7.6	Influence of Soil Depth on Draft and Pdraft for Varying Levels of Velocity	69
7.7	Draft and Pdraft Results for Optimum Combination of Factors	72
B.6.1	Soil Density Data for Varying Soil Depth	92
C.7.1	Observed and Predicted Results	94
C.7.3	Computer Printout for Analytical (Math) Model Using Minicomputer	99
C.7.4	Generated Draft and Pdraft Data for Varying Soil Depth	101
C.7.5	Generated Draft and Pdraft Data for Varying Slide Angle	107

LIST OF FIGURES

Figure		Page
2.1	Geometric Elements of an Undercutter	14
3.1	Design Parameters of an Undercutter Wing	19
4.1	Forces Acting on the Tool	24
4.2	Forces Acting on the Soil Segment	24
4.3	Mohr-Coulomb Failure Diagram	25
5.1	Views of Tillage Tool Dynamometer	31
6.1	Soil Density Variation with Depth in the Soil Bin	34
6.2	Penetrometer Pressure Variation with Depth in the Soil Bin	36
6.3	Shear Stress vs Normal Stress Curve for Direct Shear test on Artificial Soil	38
6.4	Tangential Stress vs Normal Stress Curve for Determination of Soil-metal Interface Properties in the Soil Bin	40
6.5	Calibration Curve for the Hydraulic Motor Pump on the Soil Bin	43
6.6	Twenty-nine Model Tools Designed for this Investigation	44
6.7	Laboratory Data Acquisition System	45
6.8	Schematics of Data Acquisition System	47
7.1	Soil Surface Profile for Model Tool No. 15 Operated at a Soil Depth of 1.27 cm (V = 97 cm/sec.)	50
7.2	Soil Surface Profile for Model Tool No. 15 Operated at a Soil Depth of 3.81 cm (V = 97 cm/sec.)	50
7.3	Bulldozing Effect of Tool No. 21 at a Shallow Depth (D = 1.27 cm V = 83 cm/sec.)	51
7.4	Draft and Pdraft vs Velocity for Levels of Soil Depth	60
7.5	Draft and Pdraft vs Velocity for Levels of Slide Angle	64
7.6	Draft and Pdraft vs Slide Angle for Levels of Vecocity	69
7.7	Draft and Pdraft vs Soil Depth for Levels of Velocity	71
A.4.1	Geometric Elements of a Soil Segment	90

LIST OF FREQUENTLY USED SYMBOLS

ψ = angle of soil forward failure with respect to the direction of travel of the tool.

μ = coefficient of soil frictional resistance

ϕ = angle of soil shearing resistance

μ' = coefficient of soil-metal friction

δ = soil-metal frictional angle

ρ = soil bulk volume weight (kN/m^3)

c = soil apparent cohesion (kPa)

σ = stress normal to the shear plane (kPa)

σ_1 = major principal stress on the Mohr's circle (kPa)

σ_2 = intermediate principal stress on the Mohr's circle (kPa)

σ_3 = minor principal stress on the Mohr's circle (kPa)

τ = soil shearing strength (kPa)

c_t = soil true cohesion (kPa)

σ_e = effective stress (kPa)

ϕ_t = true angle of shearing resistance

u = pore water pressure (kPa)

S_s = soil sliding stress (kPa)

Ca = adhesion (kPa)

A = area of soil forward shear failure surface (cm^2)

G = weight of soil segment (N)

B = acceleration force on soil segment (N)

2γ = nose angle of the undercutter

θ = slide angle of the undercutter

β = angle of (inclination) mounting of each wing to the horizontal plane

ϕ_w = frictional angle of weed plants on metal

$\Delta\gamma$ = correction angle for the nose angle

β_o = cutting angle of the tool

i = sharpening angle of the tool

ε = back angle of cutting or the angle of the gap

w = wing width (cm)

W = overall width of the tool (cm)

b = length of the cutting edge of each tool wing (cm)

k = pure cutting resistance of the soil (N/m)

d = depth of tool operation (cm)

v = tool velocity (m/sec. or cm/sec.)

$\vec{N}_0$ = normal force on the tool wings (N)

$\vec{N}_1$ = normal force on the soil failure surface (N)

F_x = draft force (N)

S = side draft force (N)

V = vertical force (N)

g = acceleration of gravity (m/sec^2 or cm/sec^2)

H = lift height of the tool (cm)

Chapter I

INTRODUCTION

Of the major bottlenecks in agricultral production, the problem of weed control is quite serious. In developing countries where most farms have not been completely mechanized, the problem is further compounded by the apparent lack of appropriate weed control tools. Besides, certain soil conditions require special tools for cultivation and weed control.

Loose soils are an example whereby the soil structure must be protected as weeds are being removed. The conventional methods of rotary hoeing and inter-row cultivation using small cultivator sweeps are often unsuitable for all systems of cultivation.

It is therefore not surprising that the problem of mechanical weed control in agricultural production has persistently intrigued farmers and engineers alike. The world's different systems of cultivation and soil types call for the development of relevant weed control tools adaptable to each ecological zone.

Weed control tools, like many other implements, have gone through many stages of development and modifications. The hoe is considered the earliest tool to be invented for weed control (40). The first horse drawn cultivator was invented in 1856 and tractor mounted cultivators became a reality in 1925 (46). Early cultivators were no more than pointed rods known as grubbers (3), but were quickly followed by modified forms with curved tines called scarifiers. Subsequent developments were mere improvements on the existing tools.

In order to satisfactorily accomplish the objectives of cultivation which, according to Bainer, et. al. (1), include weed control, loosening of the surface mulch and the conservation of moisture, a more suitable tool

must, of necessity, be developed for specific soil conditions. Bainer, et al also claimed that the average annual loss of crops due to weeds in the U.S.A., as estimated by USDA was in 1978 about $5 billion. About 3 billion tons of soils were eroded from the fields and pastures in 1933 and 4 billion tons in 1968, according to David, et. al. (9). Smith (41) estimated in 1968 that the annual cost of erosion control in the U.S.A. was about $4 million.

Recently, special tools that are suitable not only for inter-row cultivation but also for stubble mulch farming in loose soils have been developed. These include the undercutter cultivator sweeps. Undercutters are symmetric V-blades that operate in the soil at depths less than 25 cm. They are widely used in sandy soils of the world including the Great Plains of the U.S.A. (10). The objective of their operation is to slice through the roots of the weeds with slight lateral displacement of the soil exposing the weed roots for drying while disturbing the soil structure to a minimum. Undercutters are essentially soil cutting tools that are geometrically similar to the small arrow shaped cultivator sweeps.

Despite the increasing application of this tillage tool, a complete analysis based on its design has not been fully made. Whether the present configurations are the most effective in terms of weed control is now uncertain. Draft power requirement and minimum soil disturbance cannot be ascertained until a further study of the tool is carried out through the analysis of its geometric elements and verification with tillage experimentation.

There are, of course, inherent problems in conducting tillage research, according to Siemens (37). These include: (a) reproducing field conditions, (b) the many soil variables which often lead to complex analytical expressions if all are included in the analysis, and (c) the nature of forces on these soil working tools is not too precisely defined.

The use of artificial soils in the laboratory has, to some extent, simplified the problem of predicting the behavior of prototypes resulting from model tool designs. This is possible because of the reproducible nature of such soils. But their use has not completely eliminated the problems associated with identifying pertinent soil properties relevant to each tillage tool investigation. There is also uncertainty about how closely the use of oil, to alter the cohesive-fictional components of such soils, simulates natural soils. Despite these drawbacks, useful and reliable results have been attained with the use of artificial soils in tillage research.

Several soil properties have been identified by many authors (37,42) as being relevant to tillage tool research. These include soil cohesion, frictional angle, soil bulk density,angleofsoil-metal friction and adhesion.

The Mohr-Coulomb failure criterion or its modified form has been successfully applied to inclined and near vertical flat blades (23,37,42,47) and mathematical relationships have been developed to predict draft forces from model tool designs. The form and extent of interacting factors in these predicted relationships have, however, not been fully explained. For instance, there are inconsistencies in the soil properties identified with each tool studied. It has not been possible to establish a correlation between soil properties associated with a particular tool investigation and those needed for investigating other tools. This may be partially explained by the fact that soil is nonhomogeneous and anisotropic and its properties can therefore be easily influenced, and in fact altered, by extraneous factors. Mathematical models presuppose the inclusion of certain soil properties which need be justified or verified during experimentation.

A great deal of reliance is placed on the mechanics of tools and soils and their dynamic interactions in conducting a tillage experiment. The

use of scale models and the application of similitude techniques to the study of tillage implements under controlled environments have produced dependable results widely used in model-prototype tool predictions.

The objective of this research was to achieve better understandings of the optimum design parameters of undercutter plow sweeps through:

a) the study of the geometric elements of the tool that influence its design and application

b) identification and characterization of those soil properties pertinent to the study.

Several model tools were fabricated for this study. Emphasis was placed on the influence of soil, slide angle (θ), lift height (H), wing width (w), wing inclined angle (β), nose angle (2γ) and the overall width of the tool (W) on draft force (See Fig. 2.1 for identification of the tool parameters). Results obtained were compared with that from the mathematical model developed to see how closely the two agree.

The performance of this tool was not evaluated beyond its draft power requirement since other factors were not within the scope of this investigation. It is anticipated that future work will correlate the attained optimum design and performance characteristics with soil disturbance and weed control potentials.

Chapter II

REVIEW OF LITERATURE

2.1 Engineering Properties of Agricultural Soils

A soil subjected to compressive or tensile stress fails along definite surfaces of slip whose inclination to the principal stress are defined by the soil properties (30). This failure pattern has been applied to the study of soil engaging cultivation implements and its recognition is essential to the study and the design of agricultural implements. In the past, soil strength was related to earth dam construction and the bearing capacities for foundations, according to Tsymbal (44), but in tillage, the goal is the disruption (elastic and plastic deformations) of soils by soil engaging implements.

Osman (27), in his work on soil cutting, inferred that as a blade is moved through the soil, it compresses the soil until it reaches its maximum shear strength at which point failure occurs. This is in agreement with the Mohr-Coulomb failure criterion. According to Fountain (12), the Coulomb shear strength equation consists of two parts:

a) frictional component which is a function of the normal load,

b) cohesive component which is independent of the normal load.

These two components are vividly expressed in Coulomb's equation as follows:

$$\tau = c + \sigma \tan\phi$$

where τ = shear strength of the soil,

c = apparent cohesion, the shear strength with zero normal load,

σ = total pressure normal to the shear plane,

ϕ = angle of shearing resistance.

Fountain further stated that c and ϕ are empirical parameters of the above equation whose values hold good only under a given set of soil

and testing conditions. If a test is conducted under constant pore water pressure, the equation is modified to:

$$\tau = c_t + \sigma_e \tan \phi_t$$

where c_t = true cohesion

$\sigma_e = (\sigma - u)$ = effective pressure

ϕ_t = true angle of shearing resistance

u = pore water pressure

The normal load on the shear plane caused by the passage of any implement through the soil depends on the stress history of such soil and the size and shape of an implement.

Sineokov (39) adduced that the non-uniformity of soil structure coupled with the rapidly changing soil moisture make the study of soil strength characteristics difficult. It is known that the ultimate tensile and compressive strength of soils decrease with an increase in soil moisture content. This is particularly true for purely cohesive soils and those containing a high proportion of plant roots. The cohesion of top soils (tillage regimes) is much lower than that of subsoils of similar texture but their frictional angles are higher in magnitude.

In addition to cohesion, and the angle of shearing resistance, are the angle of soil-metal friction and adhesion. The soil-metal friction is influenced by the normal force, soil type, surface roughness and the sliding velocity of the soil along the (metal) surface (39). Gill and Vandenberg (14) explained the soil-metal friction in terms of the dynamic property of the (soil-machine) system. Sagach et. al. (34) claimed that soil-metal friction can account for about 40 to 50 percent of the total plough resistance. This value can be reduced by the presence of free water (saturation) and by the surface finish of the tool.

Soil adhesion, according to Gill and Vandenberg, is the attraction between the soil and soil engaging machine. Adhesion impairs the quality of work and increases with increases in tractive resistance, soil dispersion, contact pressure and the soil moisture (up to a limit). Soil sliding stress is computed from the soil-metal friction and adhesion as follows:

$$S_s = Ca + \sigma \tan \delta$$

where S_s = soil sliding stress

Ca = adhesion

σ = normal stress of friction surface

δ = angle of soil-metal friction

Devices used to measure soil shear properties in the field include the torsional shear box, Cohron sheargraph, cone penetrometer and annular test apparatus. The torsional shear box is commonly used for in-place topsoil strength measurements because the failure plane it induces corresponds to the surface of natural soil weakness and the shear strength is little affected by the rate of straining the soil. It is, however, not useful for determining the shear strength of soils with large stones, organic matter and roots. The Cohron sheargraph (8) is used for measuring the shear strength of the soil either in the field or in laboratory soil bins. Its action is based on the Coulomb failure theory. It is fast and dependable but it is more widely used in traction studies than in tillage research. Cone penetrometers are useful for in-place strength determinations at varying soil depths. They are being used in saturated soils subjected to compaction or traffic. Measurements are in terms of cone index or penetration resistance. They are often influenced by two factors:

i) the rate at which it penetrates the soil, generally increasing as the penetration rate is increased.

ii) The base area of the cone, high for a small cone area and low for a large cone area.

According to Schrock (36), penetration is a composite parameter whose result depends on other independent parameters such as the soil density and the soil frictional angles. In annular tests, a torque is applied to the annular sample which is strained by twisting about the principal axis of the apparatus. Its main advantage is that no change is induced in the cross sectional area of the sample during testing but it cannot be used with most agricultural soils because annular samples are difficult to attain.

The common laboratory methods for measuring soil shear strength properties, apart from those described above, are direct shear and triaxial tests. Direct shear-test apparatus has been successfully used for cohesive samples obtained from the field or on modified samples that have been given standard compaction. This method assumes failure in the horizontal plane. The triaxial test, like the direct shear test, is used for determining the soil strength properties either on cylindrical samples or on modified samples. The Mohr-Coulomb equation is the basis for shear strength determination. This compression test is achieved by making the intermediate and minor principal stresses equal ($\sigma_2 = \sigma_3$). It is also assumed that the sample is isotropic with a uniform stress distribution in all planes. Mohr stress circles can be plotted to obtain c and ϕ. Tsymbal (44) used the limiting stress approach to explain the soil failure phenomenon. The slip plane is situated at an angle $\phi/2$ to the minor principal stress. The main disadvantages of this method include, (a) the difficulty in obtaining undisturbed soil samples for the test, (b) many dry topsoils have very little strength to support them until they are loaded and stressed in the machine, and (c) the

procedure is tedious and time consuming. Siemens (37) found no significant difference between the direct shear and the triaxial shear tests and in fact recommended the direct shear test procedure due to its simplicity.

Another property used to characterize the soil is soil density. Soil density increases with soil moisture content up to a limit. An increase in bulk density has been found to increase the soil shear strength, soil frictional angles, soil cohesion and soil failure energy. Soil strength is often used to establish procedures for measuring the compaction of soils in the soil bins since there is a need to obtain uniform density with depth (37,40).

2.2 The Use of Artificial Soils in Tillage Research

Several authors (4,26,33) successfully used natural soils in their soil-machine research, but the difficulty of reproducing test conditions was serious and the rapidly changing soil moisture content often compound the problems of measuring soil properties. Bockhop (4) employed natural soil in his work with disk plows. He used colloidal properties, moisture content, organic matter composition and temperature to characterize the dynamic properties. These were found to vary widely with time. Some of the problems associated with the use of natural soils have been overcome by the use of artificial soils in laboratory soil bins.

Clark et. al. (6) identified what the characteristics of artificial soils should be:

a) strength properties should not change with time, temperature and humidity.

b) soil mix should be representative of a wide range of soil types and soil environments.

c) soil should have strength properties that can be disturbed and quickly returned to its original state without changing its properties.

d) should behave reasonably like natural soils.

The two types of artificial soils in use are the clay-sand-oil mix and the clay-sand-ethylene glycol mix. Ethylene glycol can be varied to alter the cohesive properties of the soil but it is hydroscopic (36). Spindle oil provides little change in cohesive properties but provides excellent long term stability due to slow evaporation rate.

Korayem (18) stated that the internal frictional angle generally increases with an increase in clay content but decreases with higher ethylene glycol concentrations.

The use of artificial soils is not limited to tillage-tool investigations but has been widely used for traction studies. Schrock (36) used a frictional, artificial soil consisting of 45-45-10 mix by weight of sand, clay, and mineral oil respectively. The mineral oil used is composed from Corvus mixed with Almag SAE 5-10 in ratio of 3 parts to 4 parts respectively.

2.3 Mechanics of Soil Cutting

The majority of tillage tools reported in this literature review is involved with soil cutting. Cutting is accomplished by shearing action after the soil attains maximum compressive shear strength. Plane blades, chisels, and undercutters are involved with the cutting and lifting of the soil. The failure plane established by this cutting process is referred to as the shear surface.

Designing soil cutting tools for agricultural purposes is by far one of the more complex of all engineering problems because of the variability

of soil conditions and the fact that soil is nonhomogeneous and anisotropic. Design of tillage tools is, however, based on an assumption of soil homogeneity.

Payne (30) investigated the relationships between tool geometry, speed of operation and the volume of soil upheaval using soil mechanics theory. The Mohr-Coulomb failure theory was advanced to explain soil cleavage by wide and narrow tines and he applied the passive earth pressure of Rankine to explain the soil upheaval in front of narrow tines operating at shallow depths. The failure planes he obtained for wide tines approximated straight lines whereas those for narrow tines were essentially curved. Soil-metal frictional angle was found to be independent of speed.

Kawamura (17) studied tools having various angles of inclination and operating at varying speeds and depths. He developed a mechanics theory to determine the angles of inclination corresponding to minimum draft. As his inclined tools approached the vertical plane he obtained the same result as Payne, that the shear surface was curved and that the shear angle was influenced by speed and depth of operation.

Soehne (42) studied inclined-plane blades and established an analytical procedure to determine the draft force using various soil and tool parameters. This force was made up of soil and soil-metal frictional components, shear failure, acceleration force and soil-cutting resistance respectively. Soehne inferred that for low angles of inclination (less than 40 degrees) the shear surface is not curved but a straight line, inclined at an angle of $45-\phi/2$ to the horizontal. Soehne found that frictional force due to lifting of the soil was higher than other frictional components but the force for accelerating the soil segments was negligible. Maximum cutting resistance occurred between 11 and 15 degrees of inclination angle.

McKyes, et. al. (24) used the equilibrium mechanics approach to develop a mathematical model for inclined narrow blades. This approach was based on straight-line failure planes and is a simplified and advantageous method compared with the log-spiral method for curved failure planes reported by Payne. Draft force was observed to increase with increases in rake (lift) angles, for a given depth to width ratio, in the same soil condition. Field results were in agreement with the model. Osman (27) investigated the influence of curvature of soil cutting blades on draft by using the Coulomb equation to develop his theory based on the passive earth pressure and Ohde's graphical logarithmic spiral. Dimensional analysis was used to handle the large number of variables. Osman showed that draft force increases with increases in rake angles for angles greater than 30 degrees. At low rake angles and under the same soil conditions, the draft forces for flat and curved blades were almost equal but the manner of soil movement on each blade type was different.

Luth and Wismer (23,47) continued with the work of Soehne and Kawamura. Various lift angles and widths of inclined tools were investigated in purely frictional and purely cohesive soils. Results obtained were comparable with earlier work on this tool type.

2.4 Tillage Sweep Design

Information currently obtainable on tillage sweeps deal more with their application than with their optimum design characteristics. In the past, practical knowledge of plane blades was utilized in the fabrication of this tool type but recently, the need to optimize their design to achieve better performance has necessitated further theoretical development. This, coupled with the need for effective weed control on lands prone to wind erosion, led to the design and manufacture of large sweeps called undercutters.

Sirohi (40) studied the influence of the geometric elements of several sweeps on draft. The influence of slide angle, nose angle, tool width and tool surface area on draft force were studied. The optimum slide angle was found to occur between 13 and 15 degrees for the range of speeds used. This result is in close agreement with what was obtained for plane blades (23,42,47). The nose angle was found to influence the slide angle and the surface area of each tool. The nose and slide angles investigated were within the ranges of 60 and 120 degrees and 4.5 and 31 degrees respectively. Only nose angles between 60 and 100 degrees were used to establish the functional relationships for the draft force. The overall widths of the tools varied between 102mm. and 508mm., but the lift height was fixed for all tools. The maximum velocity was about 15.84 km/hr.

Several Russian authors have researched basic design parameters for tillage sweeps. Sineokov (38) pioneered the development of design parameters for cultivator sweeps for use in soil loosening and in removal of weed plants by means of undercutting. The designs of arrow-shaped undercutting sweeps were based on the nose angle (2γ), angle of mounting of the wings to the horizontal plane (β), slide angle (θ), wing width (w), and the overall width (W) of the tool (Fig. 2.1). He selected the nose angle based on the frictional angles of weed plants on metal, ϕ_w, along the cutting edge of the tool. He said that if $\gamma < (90-\phi w)$ there is undercutting of weeds but if $\gamma > (90-\phi w)$ clogging of the cutting edge would result. From his experimental work he found this frictional angle to lie between 22 and 45 degrees. This mathematical relationship was widely accepted and used by other Russian researchers.

Tsymbal (43) however argued that it is the soil-metal frictional angle, δ, and not that of weeds on metal that should be used in this

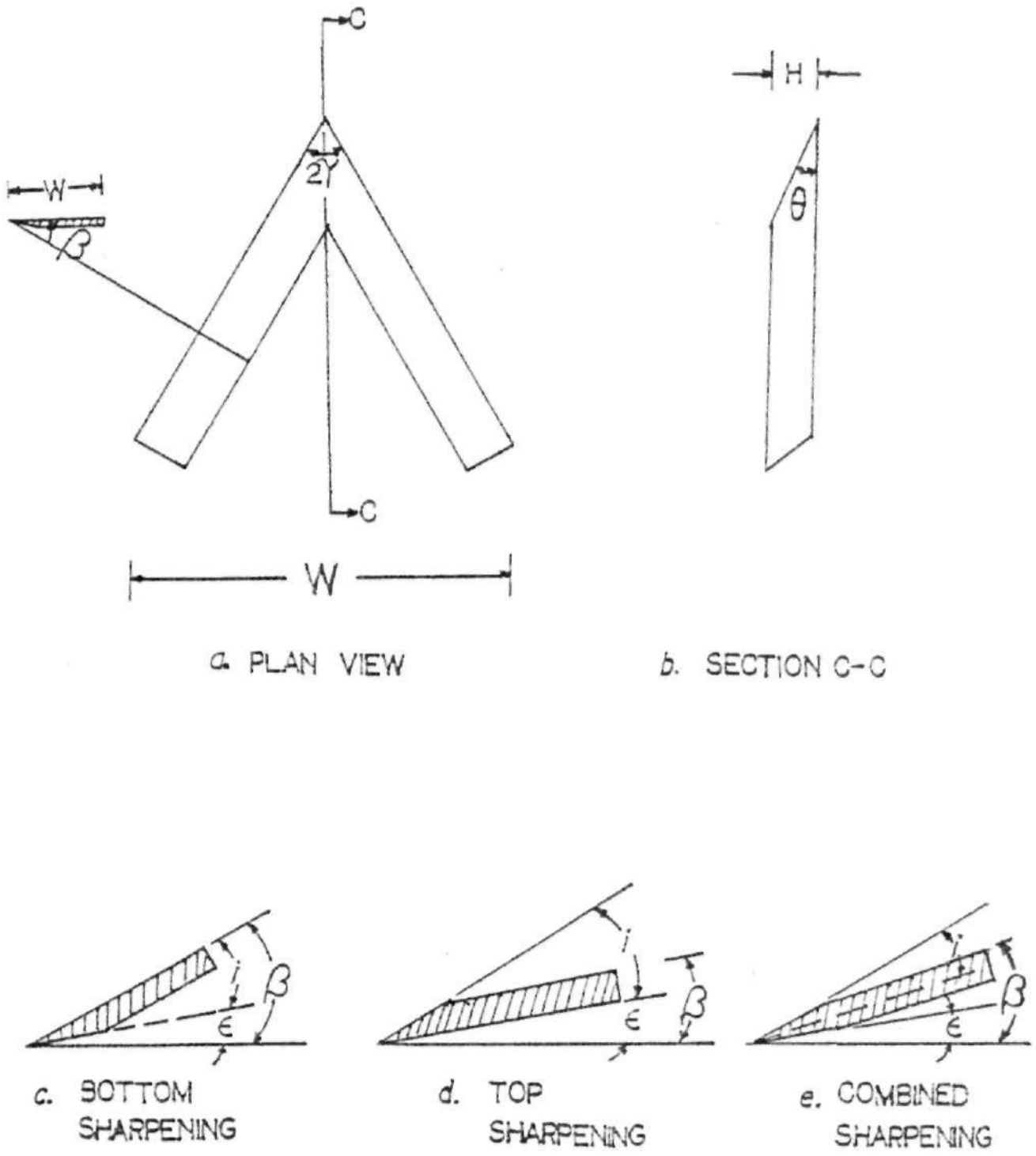

Fig. 2.1 Geometric Elements of an Undercutter

relationship. This is because of the predominance of soil in the soil mass containing weeds, and as such the coefficient of the weed stems on steel is always less than that of soil on steel. Moreover, the weeds in a soil mass cannot slide off the cutting edge earlier than the soil. He therefore modified the established relationship to:

$$2\gamma \leq 2(90 - \delta) - \Delta\gamma$$

where $\Delta\gamma$ = correction angle = 10°

This modified equation guarantees the sliding of soil and weeds along the cutting edge and it is most applicable to the design for optimum nose angles of undercutter sweeps.

Another parameter investigated was the angle of mounting of the wing planes to the horizontal plane, β. For good undercutting of weeds, the angle of cutting, β_o, must be minimal. β_o is defined as:

$$\beta_o = i + \varepsilon$$

where i = the sharpening angle of the tool

ε = the back angle of cutting or the angle of the gap

Sineokov used β to determine the amount of crumbling or fragmentation caused by the sweep. He found that its selection is related to soil type and the nature of cutting edge sharpening. For β less than 15 degrees, it is recommended that the sharpening should be at the top face of the wings. Combined sharpening is recommended for β between 15 and 25 degrees, and sharpening should be on the bottom when β is greater than 25 degrees (Fig. 2.1). It has been established that the soil moves parallel to the direction of forward travel of sweeps, along the sweep's slide angle. This observation is significant to the study of the acceleration and frictional forces. The optimum combination of these tool parameters depends on the amount of soil crumbling desired and the draft force.

2.5 Application of Similitude Techniques to Tillage Research

In recent years, the similitude approach to scale-model testing for the prediction of prototype tillage tool performance has become very popular. This approach has to a great extent simplified the otherwise complex procedure of developing functional relations for model-prototype designs.

Similitude techniques, according to Freitag (13), are based on the concept of similarity between a model and a prototype. Two systems are deemed similar if they exhibit geometric, kinematic and dynamic similarities. Geometric similarity is achieved if the two systems are geometrically proportional. Dynamic similarity is achieved if the ratio of forces are the same in the two systems. If geometric and dynamic similarities are achieved then kinematic similarity is, by implication, achieved.

Forces affecting dynamic systems can be identified by constructing a set of dimensionless groups for all system variables with each having equal values in both the model and the prototype. Schafer et. al. (35) stated that for accurate prediction of a prototype tool from a model tool, all variables must be included in the prediction equation and the model design conditions must be satisfied. Failure to achieve equality in one or more design conditions would lead to a distortion of the system.

The inability of the researchers to scale soil variables often leads to distorted models in soil-machine systems. One way of minimizing this problem is by using the same soil for testing both the model and the prototype and explaining the results on the basis of this known phenomenon. The use of dimensional analysis permits the grouping of variables into dimensionless pi terms in accordance with the established

model theory (21,25). The model theory requires that the corresponding pi terms in the model and prototype be equal or scaled to achieve this equality. Schafer et al (35) proposed ways of achieving this equality analytically, experimentally or by using compensated model techniques.

Several tillage researchers have in the past applied similitude techniques to their tillage investigations. Bockhop (4) used this technique in his model-prototype study of disk plows. Other researchers (2,22,45) used distortion factors to determine the magnitude of predictive factors needed to achieve reasonable predictions of tool forces.

The wide application of this technique and its success devolve on the ability of the researchers to characterize and measure pertinent soil variables which often cause distortion.

Chapter III

DESIGN EQUATIONS FOR UNDERCUTTER BLADES

Vector mechanics has been applied in developing the design equations for the undercutter wings. For these derivations, it was assumed that two of the geometric elements ($\gamma,\theta,\beta,\alpha$) are known while the others were developed in terms of these two. It makes no difference which two design parameters were selected for starting as each parameter has a functional relationship with the other.

Due to the symmetry of undercutter-sweeps, one wing can be used to establish the design equations. The angle between the wing of the tool and the xy (horizontal) plane, defined by β, can be redefined in terms of γ and θ, thus:

a) $\beta = f_1\ (\gamma,\theta)$

From Fig. 3.1(a), the vectors A and B and be defined as:

$$\bar{A} = \begin{Bmatrix} -\cos\gamma \\ \sin\gamma \\ 0 \end{Bmatrix} \quad \text{and} \quad \bar{B} = \begin{Bmatrix} -\cos\theta \\ 0 \\ \sin\theta \end{Bmatrix}$$

The cross product between $\bar{A}$ and $\bar{B}$ ($\bar{A} \times \bar{B}$) is perpendicular to the plane of the wing as shown in Fig. 3.1(b). The components of vector C in the x, y and z directions are:

$$\bar{C} = \bar{A} \times \bar{B} = \begin{Bmatrix} \hat{i} & \hat{j} & \hat{k} \\ -\cos\gamma & \sin\gamma & 0 \\ -\cos\theta & 0 & \sin\theta \end{Bmatrix} = \begin{Bmatrix} \sin\gamma\sin\theta \\ \cos\gamma\sin\theta \\ \sin\gamma\cos\theta \end{Bmatrix} \quad \begin{Bmatrix} x \\ y \\ z \end{Bmatrix}$$

$\cos\beta$ is the z component of $\bar{C}$ divided by the magnitude of $\bar{C}$:

$$\cos\beta = \frac{\bar{C}_z}{|\bar{C}|} = \frac{\sin\gamma\cos\theta}{(\sin^2\theta+\sin^2\gamma+\cos^2\theta)^{1/2}}$$

and

$$\beta = \cos^{-1}\left\{ \frac{\sin\gamma\cos\theta}{(\sin^2\theta+\sin^2\gamma+\cos^2\theta)^{1/2}} \right\} \qquad \text{(i)}$$

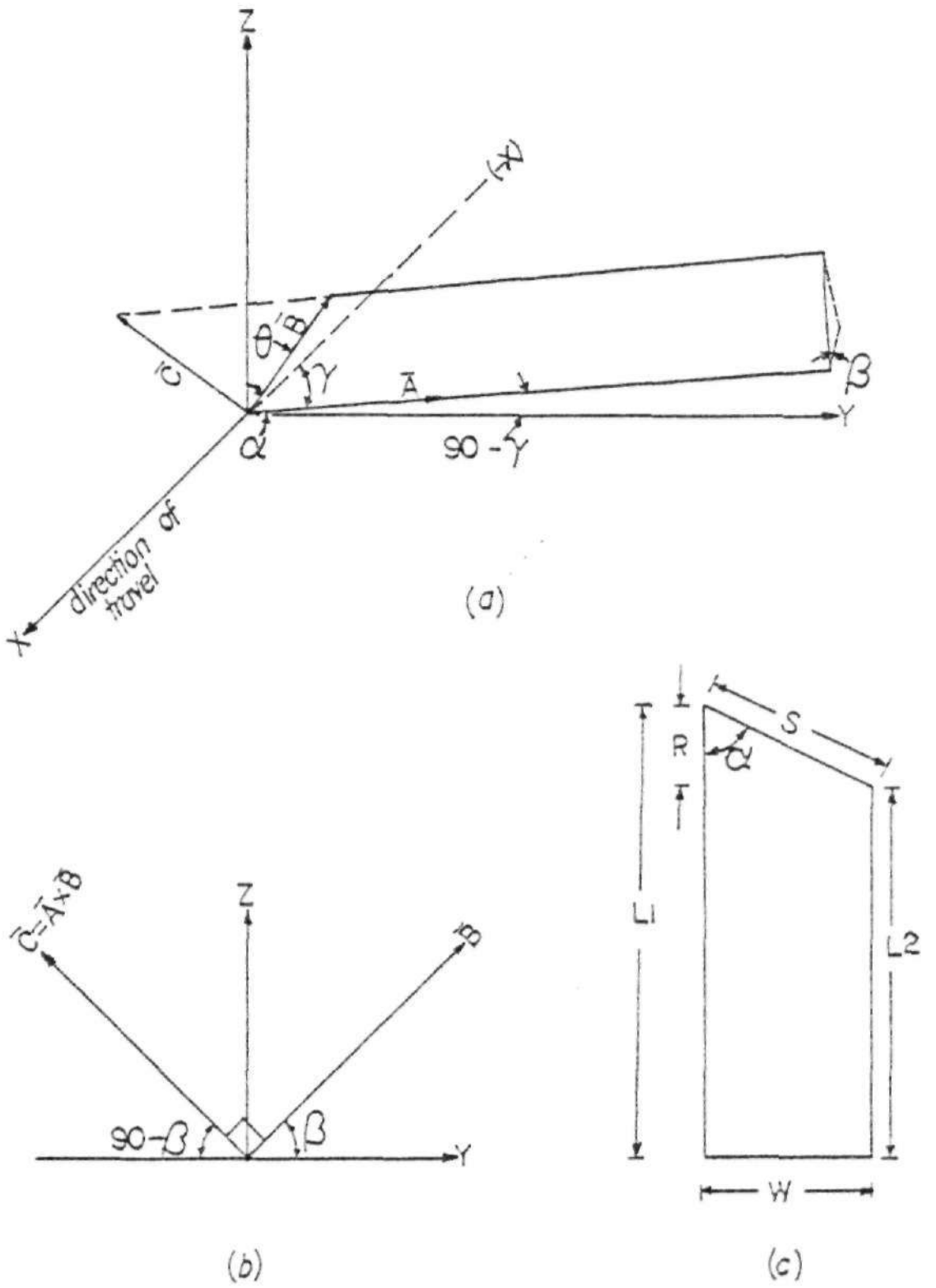

Fig. 3.1 Design Parameters of an Undercutter Wing

Similarly, $\sin\alpha$ is the magnitude of $\bar{C}$:

$$\sin\ \alpha = (\sin^2\gamma\sin^2\theta+\cos^2\gamma\sin^2\theta+\sin^2\gamma\cos^2\theta)^{1/2}$$

$$\alpha = \sin^{-1}(\sin^2\theta+\sin^2\gamma\cos^2\theta)^{1/2} \qquad \text{(ii)}$$

b) $\alpha = f_2\ (\gamma,\beta)$

A shown above,

$$\sin\alpha = (\sin^2\theta+\sin^2\gamma\cos^2\theta)^{1/2}$$

$$\alpha = \sin^{-1}(1-\cos^2\gamma\cos^2\theta)^{1/2} \qquad \text{(iii)}$$

and

$$\cos\beta = \frac{\sin\gamma\cos\theta}{(1-\cos^2\gamma\cos^2\theta)^{1/2}}$$

$$\cos^2\beta = \frac{\sin^2\gamma\cos^2\theta}{1-\cos^2\gamma\cos^2\theta}$$

hence

$$\cos^2\theta = \frac{\cos^2\beta}{(\cos^2\beta\cos^2\gamma+\sin^2\gamma)} \qquad \text{(iv)}$$

Substituting (iv) into (iii) yields:

$$\alpha = \sin^{-1}\left\{\frac{\cos^2\beta\cos^2\gamma+\sin^2\gamma-\cos^2\gamma\cos^2\beta}{\cos^2\beta\cos^2\gamma+\sin^2\gamma}\right\}^{1/2}$$

$$\alpha = \sin^{-1}\left\{\frac{\sin\gamma}{(\cos^2\beta\cos^2\gamma+\sin^2\gamma)^{1/2}}\right\}$$

or $$\alpha = \sin^{-1}\left\{\frac{\tan\gamma}{(\cos^2\beta+\tan^2\gamma)^{1/2}}\right\}$$

Using the above relationships and Figures 2.1 and 3.1 respectively, other pertinent relationships can be established as shown below:

Given the lift height of the tool, H, and the tool width, W:

the wing width, $w = H/\sin\beta$

the slide length, $S = w/\sin\alpha$

the major length, $L_1 = W/2.\sin\gamma$

the minor length, $L_2 = L_1 - w/\tan\alpha = L_1 - R$

the surface area of the wing,

$$Aw = 1/2\ \{(L_1 + L_2)w\}$$

and

the total surface area, $A_t = 2Aw$

where $R = w/\tan\alpha = S\cos\alpha$

The above derivations are those that are required for designing an undercutter with the geometric shape illustrated. As the geometry of the tool changes, the pertinent equations would need to be adjusted accordingly.

The geometric elements of each model tool designed were taken into consideration in designing for its sharpening angle and its back clearance angle as shown in Fig. 2.1. The design criterion was such that the optimum back clearance angle, ε, was maintained ($\varepsilon \geq 10^{\circ}$). A minimum thickness of 1.25 mm was maintained for the cutting edge of each wing.

Chapter IV

MATHEMATICAL MODEL

The development of a theoretical model for predicting draft forces on undercutters is based on the symmetry of the tool. The theory of mechanics of equilibrium has been applied by many authors to the development of equilibrium equations for predicting forces on soil cutting tools and the results obtained were in most cases in close agreement with the experimental results. This procedure assumes a prior knowledge of the type of failure surface on the soil segments being sheared. The draft force on a soil segment is usually determined from an equilibrium analysis involving the angle of inclination of the soil shear surface, ψ, and such relevant soil properties as the frictional angles (soil on soil and soil on metal), soil cohesion and soil bulk volume weight. The geometric elements of the tillage tool and the location of the forces acting on the tool are important for establishing the equations. Vector algebra was employed by Clark, et. al. (7) in developing mathematical analysis for plan undercutting blades. This approach greatly simplified the complexity of the analytical procedure.

As a soil cutting tool moves through the soil, the soil compresses until failure results according to the Coulomb equation. The failure plane is situated at an angle of $(90 - \phi)$ to the minor principal stress plane along a path of least resistance (Fig. 4.3b). This failure angle is $(45 - \phi/2)$ to the minor principal stress plane on the soil segment.

The equilibrium equations for the undercutter can be established by applying vector algebra to the three dimensional analysis of the forces on the tool and the soil segment respectively.

4.1 Forces on the Tool

If the soil is assumed to slide parallel to the direction of travel, along the slide angle, θ, then the force components are those shown below as illustrated in Figure 4.1.

Horizontal force components: $-kb\cos\gamma$, $-\mu'\vec{N}_0\cos\theta$

Side force components: $-kb\sin\gamma$, $kb\sin\theta$

Vertical force component: $\mu'\vec{N}_0\sin\theta$

and the equilibrium force equations are:

Horizontal force: $$F_x = \frac{\vec{N}_0}{(1+\tan^2\gamma+\cot^2\theta)^{1/2}} + \vec{N}_0\cos\theta + kb\cos\gamma \qquad (1a)$$

Side force: $$S = \frac{\vec{N}_0\tan\gamma}{(1+\tan^2\gamma+\cot^2\theta)^{1/2}} + kb\sin\gamma \qquad (2a)$$

Vertical force: $$V = \frac{\vec{N}\cot\theta}{(1+\tan^2\gamma+\cot^2\theta)^{1/2}} - \mu'\vec{N}_0\sin\theta \qquad (3a)$$

4.2 Forces on the Soil Segment

The force components on the soil segment can be obtained from Fig. 4.2 and by writing the equilibrium equations as follows:

Horizontal force: $$F_x = \frac{\vec{N}_1}{(1+\tan^2\gamma+\cot^2\psi)^{1/2}} + B\cos\psi + \mu\vec{N}_1\cos\psi + cA\cos\psi \qquad (1b)$$

Side force: $$S = \frac{\vec{N}_1\tan\gamma}{(1+\tan^2\gamma+\cot^2\psi)^{1/2}} + kb\sin\gamma \qquad (2b)$$

Vertical force: $$V = G + B\sin\psi + \mu\vec{N}_1\sin\psi + cA\sin\psi - \frac{\vec{N}_1\cot\psi}{(1+\tan^2\gamma+\cot^2\psi)^{1/2}} \qquad (3b)$$

The cutting resistance components can be obtained from equations (2a) and (2b) as follows:

$$kb\sin\gamma = \tan\gamma\left\{\frac{\vec{N}_1}{(1+\tan^2\gamma+\cot^2\psi)^{1/2}} - \frac{\vec{N}_0}{(1+\tan^2\gamma+\cot^2\theta)^{1/2}}\right\}$$

and

$$kb\cos = \left\{\frac{\vec{N}_1}{(1+\tan^2\gamma+\cot^2\psi)^{1/2}} - \frac{\vec{N}_0}{(1+\tan^2\gamma+\cot^2\theta)^{1/2}}\right\} \qquad (4)$$

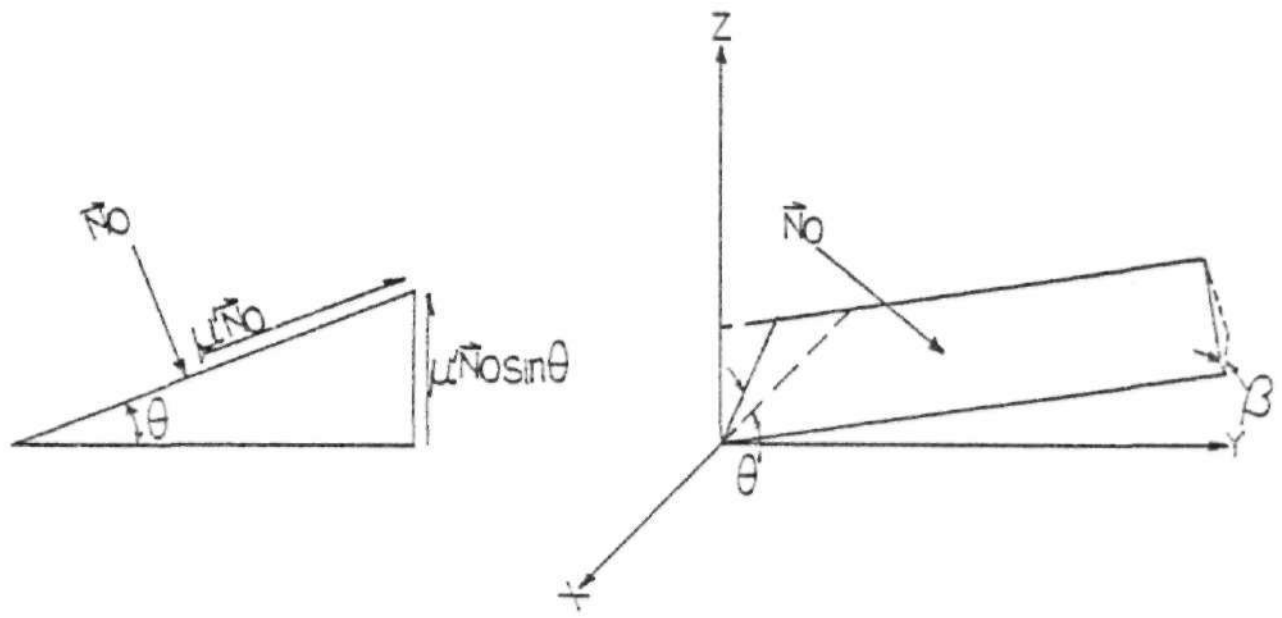

Fig. 4.1 Forces Acting on the Tool

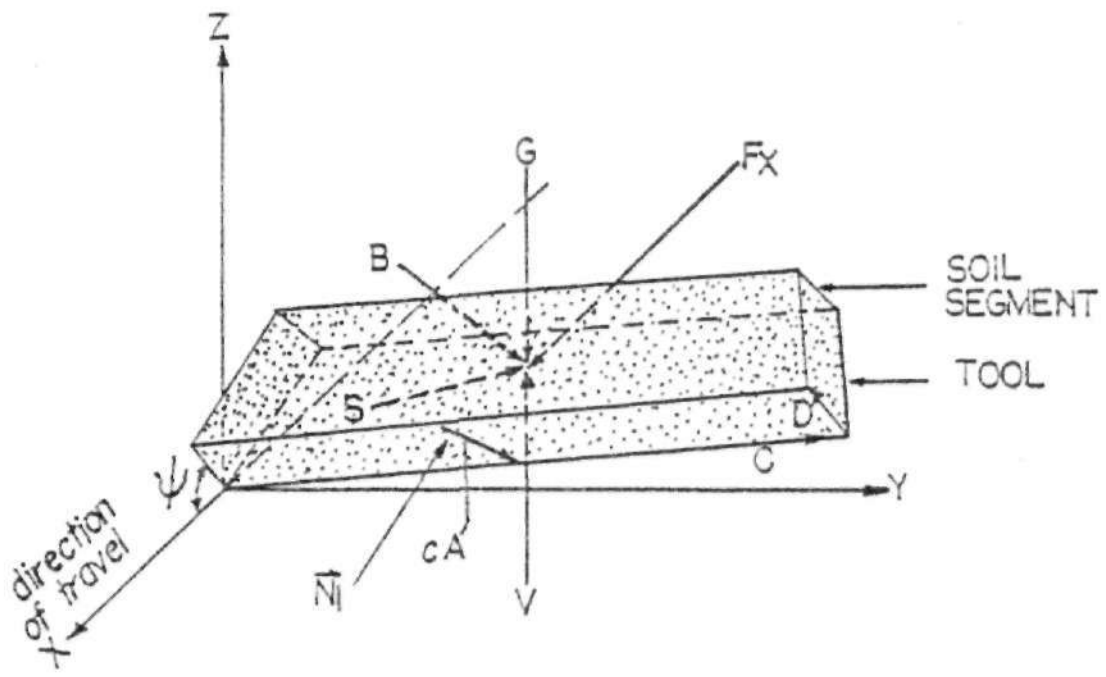

Fig. 4.2 Forces Acting on the Soil Segment

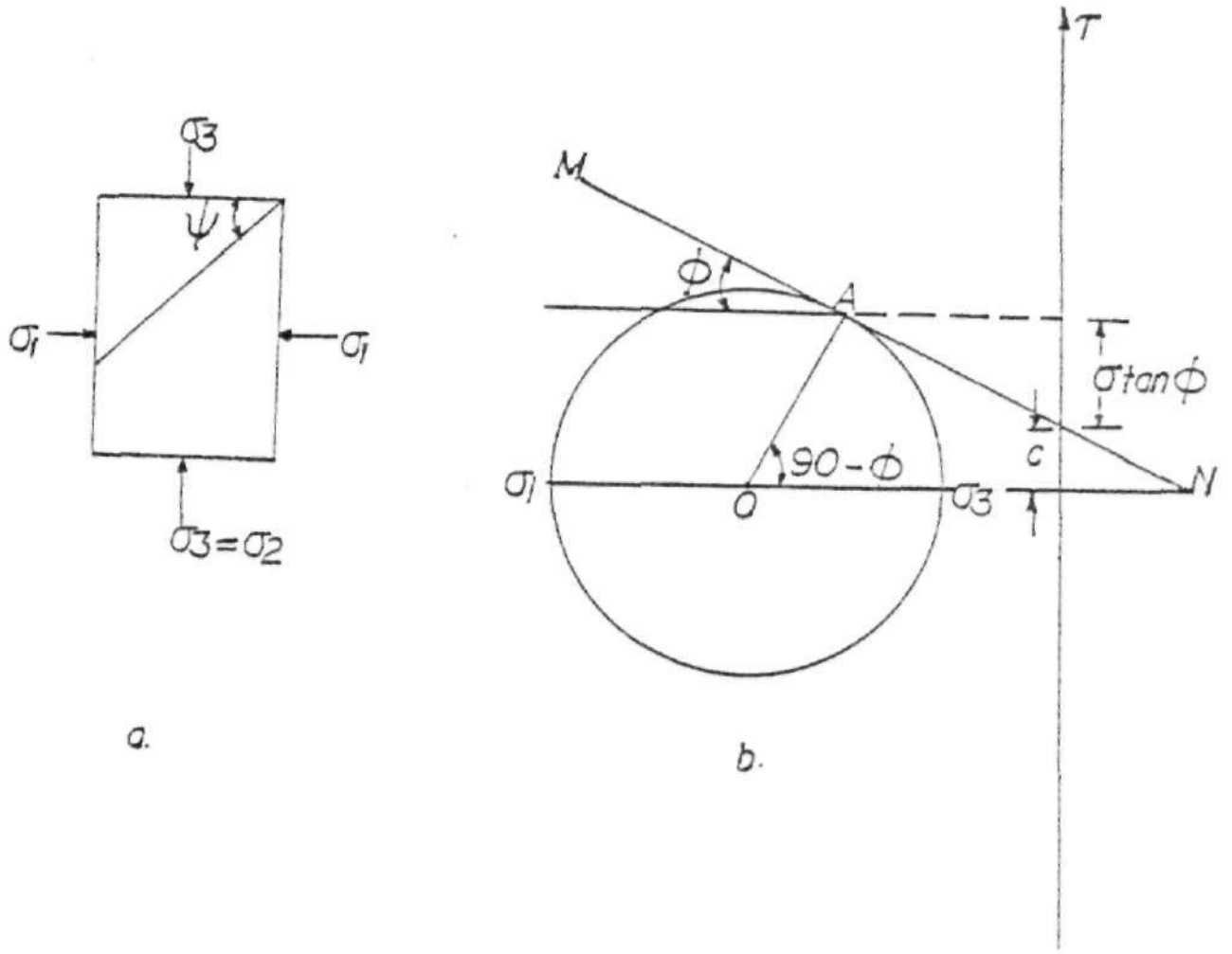

Fig. 4.3 Mohr-Coulomb Failure Diagram

The normal force on the tool, $\vec{N}_0$, can be solved for from equations (1a) and (4) as follows:

$$\vec{N}_0 = \frac{1}{\mu' \cos\theta} \left\{ F_x - \frac{\vec{N}_1}{(1+\tan^2\gamma+\cot^2\psi)^{1/2}} \right\}$$

The normal force on the soil segment is again obtained by rearranging equation (1b):

$$\vec{N}_1 = F_x - \frac{(B + cA)\cos\psi}{\frac{1}{1+\tan^2\gamma+\cot^2\psi)^{1/2}} + \mu\cos\psi} \tag{6}$$

4.2 Draft Force

From the above equations, the final expression for the draft force can be obtained as given below:

$$F_x = \frac{2}{Z} \left\{ G + (B + cA)\cos\psi \left\{ \tan\psi - \frac{\cot\theta - \mu'\sin\theta(1+\tan^2\gamma+\cot^2\theta)^{1/2}}{(\mu'\cos\theta+\mu'\cos\theta\,\mu\cos\psi(1+\tan^2\gamma+\cot^2\psi)^{1/2}(1+\tan^2\gamma+\cot^2\theta)^{1/2})} + \frac{\cot\psi - \mu\sin\psi(1+\tan^2\gamma+\cot^2\psi)^{1/2}}{\mu'\cos\theta(1+\mu\cos\psi(1+\tan^2\gamma+\cot^2\psi)^{1/2})} \right\} \right\} \tag{7}$$

where

$$Z = \left\{ \frac{\cot\theta - \mu'\sin\theta(1+\tan^2\gamma+\cot^2\theta)^{1/2}}{\mu'\cos\theta(1+\tan^2\gamma+\cot^2\theta)^{1/2}} + \left\{ \frac{\cot\psi - \mu\sin\psi(1+\tan^2\gamma+\cot^2\psi)^{1/2}}{\mu'\cos\theta(1+\mu\cos\psi(1+\tan^2\gamma+\cot^2\psi)^{1/2})} \right\} - \frac{\cot\theta - \mu'\sin\theta(1+\tan^2\gamma+\cot^2\theta)^{1/2}}{(1+\tan^2\gamma+\cot^2\theta)^{1/2}\,(\mu'\cos\theta+\mu'\cos\theta\,\mu\cos\psi(1+\tan^2\gamma+\cot^2\psi)^{1/2}} \right\}$$

The approach described by Soehne (42) was used for obtaining the weight of the soil segment and the acceleration force on the soil segment respectively as follows:

Weight of the soil segment;

$$G = \rho b \frac{d\sin(\psi+\theta)}{\sin\psi} \left\{ w + d/2 \left\{ \frac{\cos(\psi+\theta)}{\sin\psi} + \frac{\sin(\psi+\theta)\tan\theta}{\sin\psi} \right\} \right\}$$

The failure surface area,

$$A = \frac{bd}{\sin\psi}$$

and

acceleration force;

$$B = \rho/g \; b \; d \; v^2 \frac{\sin\theta}{\sin(\psi+\theta)}$$

Details of this mathematical model are given in the appendix. Equation (7) was verified experimentally to see how closely the theoretical model predicted draft force on the undercutters designed.

Chapter V

EQUIPMENT DESIGN

The soil bin facility employed for this investigation consists of the following

1. The test (artificial) soil
2. The soil trough (container)
3. The soil processing carriage
4. The test tool dynamometer carriage
5. The test tools

The test soil is an artificial soil consisting of a mixture of "#520 Oregon Silica" sand, "fire" clay supplied by Hill & Griffith Co., Chicago, IL, and mineral oil (a mixture of "Corvus" and "Almag") in the ratio of 45-45-10 by weight as reported by Schrock (36).

The soil trough was constructed of concrete. It is 15.2 meters long, 114 cm wide and 60 cm deep. Soil depth is about 40 cm.

The soil processing carriage consists of a rotarytiller, a strike-off blade and a surface roller. The raising and lowering of each component is by a hydraulic cylinder. The rotarytiller is a modified Howard Rotovator powered by a 15 kW., three phase electric motor. Its depth of operation can be varied by means of a hydraulic cylinder. The strike-off blade is mounted between the rotarytiller and the surface roller and serves to level the soil after rotarytilling. Its action is also controlled by a hydraulic cylinder. The surface roller consists of a cylindrical drum which compacts the soil by rolling over it repeatedly. This liquid tight drum is 91 cm in diameter and 110 cm long with an effective weight of 415 kg.

The carriage is pulled by a cable by a hydraulic-motor-driven winch. The winch motor is powered by a pressure compensated pump.

The speed of the motor is controlled by a flow control valve which allows for the selection of speeds between 70 cm/sec and 150 cm/sec. The initial drive cable was 5 mm. (3/16") in diameter but had to be replaced with a 6.35 mm. (1/4") diameter cable due to wear and tear.

The test wheel carriage reported by Schrock (36) was modified to carry the test tool dynamometer. It consists of

a) The rectangular steel tubing frames

b) The dynamometer

c) The tool holder

The rectangular steel tubing frames consist of the base frame which rests on the rails of the soil bin track and is pulled along these rails by the cable drive system. This base frame is provided with solid nylon tire rollers that run at the top, the side and the underside of the rails to provide for the stability and constraint of the carriage. The vertical frame that supports the dynamometer is supported by a pair of Thompson 1060 stainless steel shafts and linear bearing blocks that are bolted on to the base frame. Also bolted to the vertical frame are 32 mm (I.D.) SB-20 shaft support blocks which in turn support two 1060 stainless steel solid shafts. Each shaft is 152 cm long and 32 mm in diameter. These two shafts run across the width of the soil bin and carry the dynamometer through two rectangular tubing frames that are attached to these shafts by means of adjustable ball bushing pillow blocks.

These horizontal shafts also permit lateral movement of the dynamometer across the soil bin. This lateral movement is provided by a CMM-2710 Duff-Norton maxi-pac machine screw type mechanical actuator. Attached to the dynamometer frame through another set of shaft support blocks are two 122 cm solid shafts. These vertical shafts carry the dynamometer which can be lowered into or raised from the soil along these solid shafts by means of a Duff-Norton mini-pac mechanical actuator.

The dynamometer back plate is 2.54 cm thick aluminum. The dynamometer outer (inverted T) frame is bolted to this back plate. Along the vertical face of the inner (inverted T) frame are provisions for bolting the tool holder to the dynamometer. Mounted between the inner and outer (inverted T) frames are the six load cells and their flexures. Three of the load cells are oriented in the horizontal plane, two in the vertical plane and one in the side plane. Four of the load cells were obtained from Transducers Inc. One of these Model 182 tension load cells is rated at 4450 newtons (N) while the remaining three are each rated at 2225 N in capacity. The remaining two load cells were obtained from GSE Inc. These Model 5350 cells are each rated at 4450 N capacity. The entire arrangement is similar to that which exists in the Deere and Company soil bin.

The test tools were constructed from 3.2 mm (1/8") thick cold rolled steel. There is a universal standard which can be bolted to each undercutter tool platform by means of two 4.8 mm. (3/16") bolts. The standard is bolted to the dynamometer tool holder as shown in Fig.5.1.

The method of welding the platform to the underside of the upper junction of the wings of each tool and supported by cross braces as reported by Sirohi (40) was found to be unsatisfactory because of its effect on soil sliding friction. This was particularly true for those tools with small slide angles. This problem was resolved by using a triangular platform. Each model tool has its own platform spot-welded between the two wings and recessed about a quarter of the width of the wing from the upper edges of the wings. This reduces contact between the soil surface and the underside of the platforms and hence minimizes any soil-metal friction and adhesion which would otherwise result.

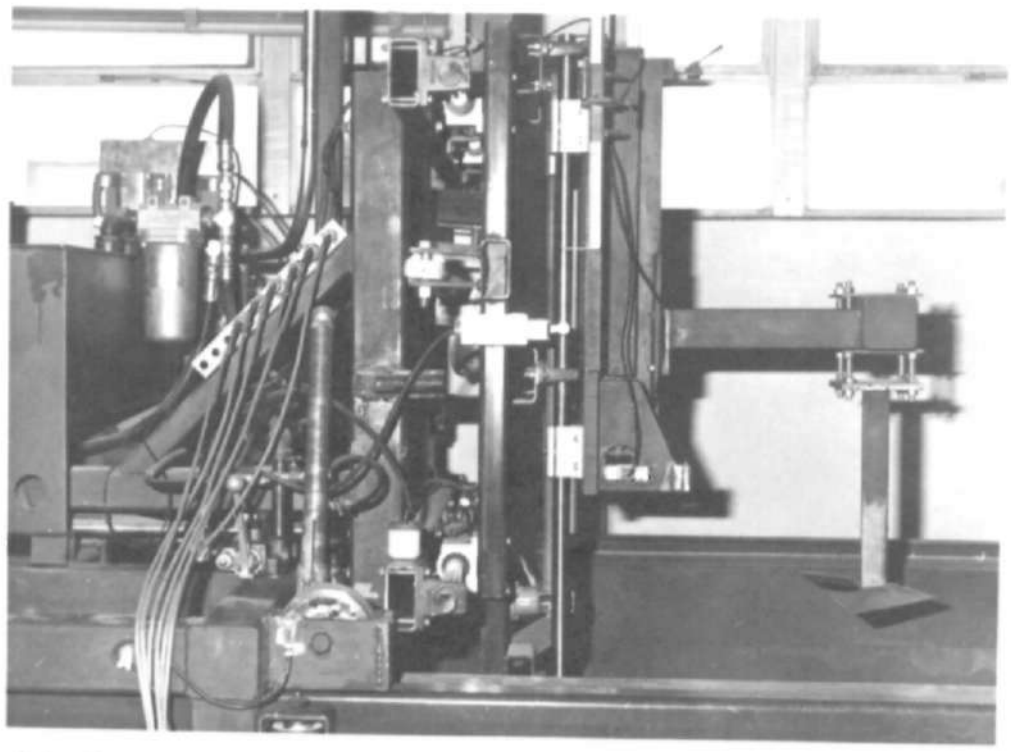

(a) Side View

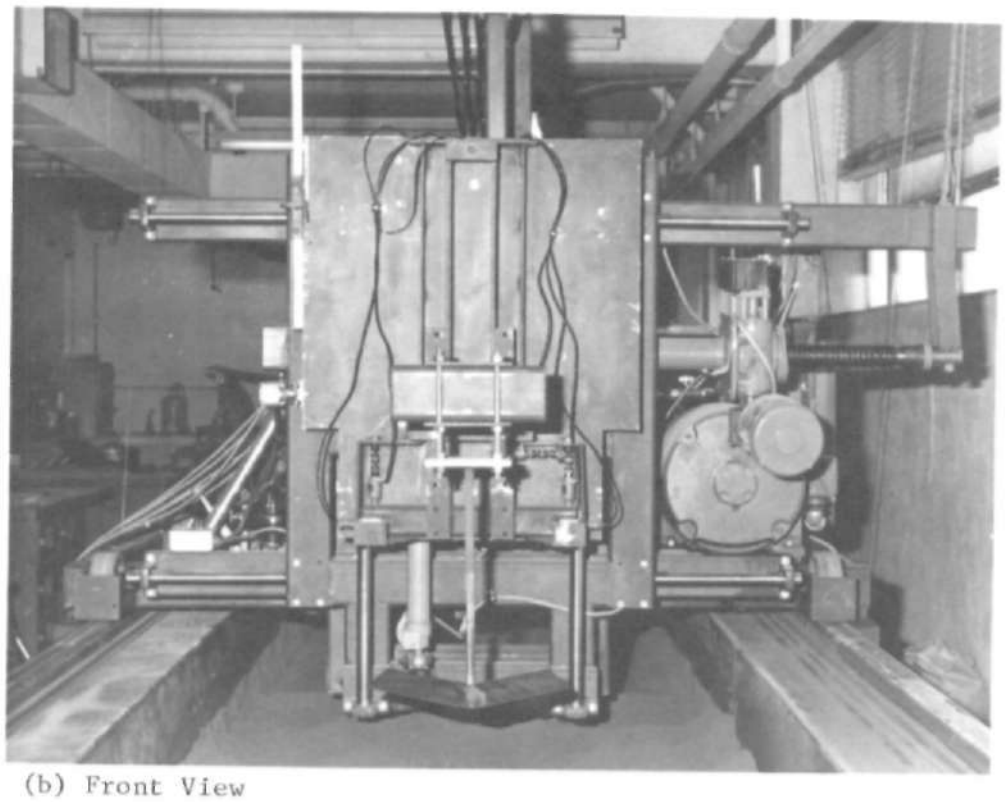

(b) Front View

Fig. 5.1 Views of Tillage Tool Dynamometer

The surface area of each platform was minimized but sufficient to position the base of the standard. Two 14.3 mm. (9/16") holes were drilled into each platform parallel to the midrib of each tool. These holes were for bolting the standard to the model tool. The overburden pressure resulting from the accumulation of soil on the platform around the standard could not be completely eliminated without unduely weakening this support and hence is thought to have contributed in some way to the observed draft forces. This was particularly true for those tools with large nose angles and those operating at greater depths.

Chapter VI

EXPERIMENTAL PROCEDURE

6.1 Soil Preparation:

Before any experimental data could be collected on the designed model tools, it was necessary to establish a consistent soil testing procedure and environment. This was achieved by processing the soil in such a way that minimum variation in soil density existed within the bin and within the range of soil depths of interest. Schrock (36) observed some density variations across the soil bin but noted that the variation along the bin was very small. Preliminary investigations confirmed these claims, hence attempts were made to establish a testing procedure that would further minimize the variations across the bin.

The soil was rotary tilled to a depth of 27 cm. The surface was leveled with a levelling blade and rotarytilled a second time to the same depth. The second rotarytilling was followed by the levelling blade. The soil density was then measured at three locations across the bin, 30 cm apart, and along the bin at six locations, 60 cm apart. The Standard Test Method for Density of Soil in Place by the Drive Cylinder Method (ANSI/ASTM D 2937-71) was adopted. A set of cylinders were constructed to remove soil cores from the surface down to a depth of 15 cm in 2.5 cm increments. The soil processing was subsequently repeated and followed by roller passes ranging from one pass to five passes with the soil density measurement taken for each level of compaction. The results of the soil density tests are shown in Fig. 6.1.

6.2 Soil Strength Properties:

Soil strength properties are important to this study from the standpoint of the theoretical analysis where cohesion, coefficient of soil

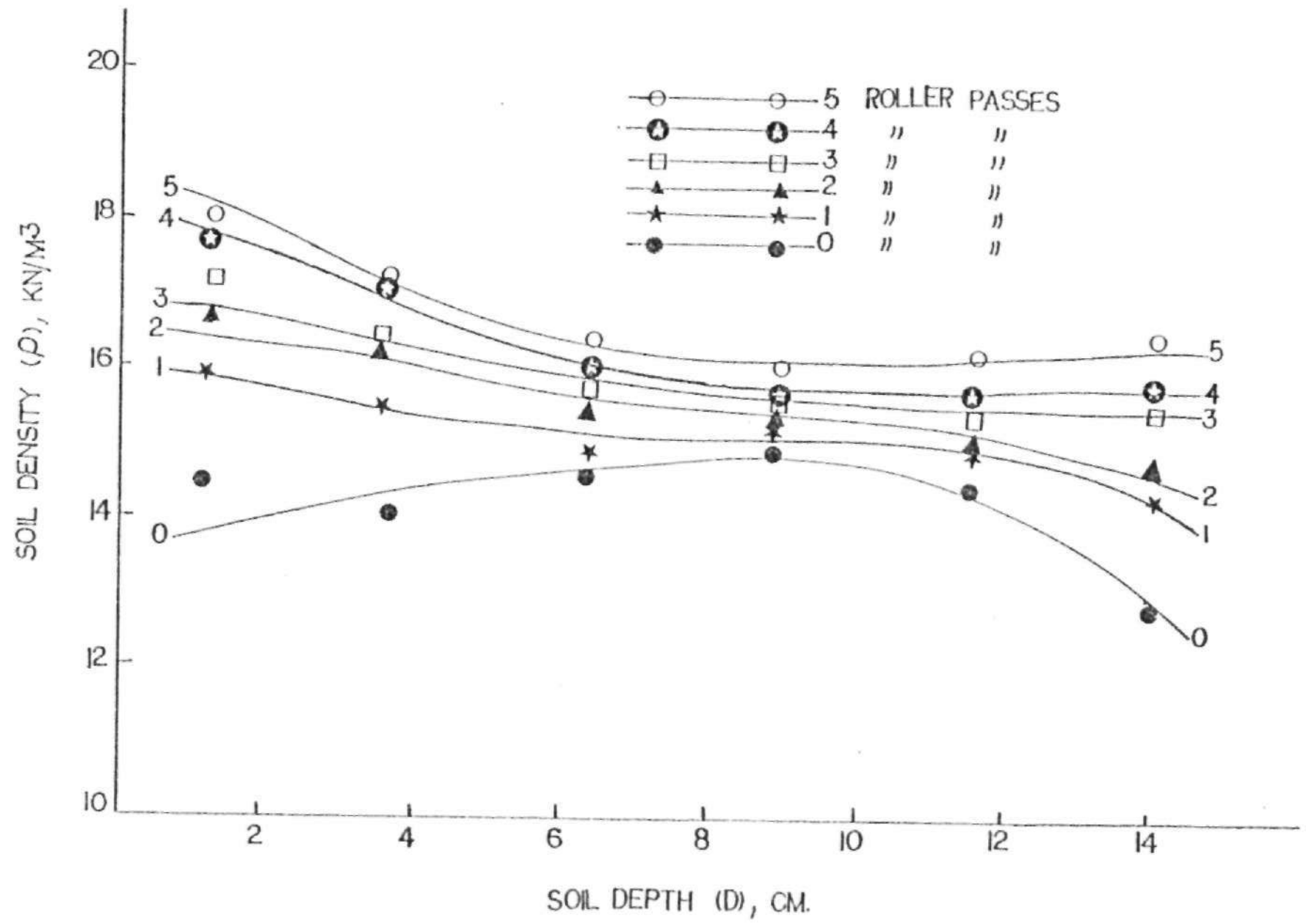

Fig. 6.1 Soil Density Variation with Depth in the Soil Bin

TABLE 6.1

Results of the Periodic Soil Property Tests
Each Value is the Average of Three Readings.

Test Conducted Prior to Test Run No.	Penetrometer Pressures (kPa) Soil, Depth, cm			Soil Cohesion c(kPa)	Soil Frictional Angle (Ø)
10	554.27	765.18	774.01	6.25	29.40
29	557.21	776.95	776.95	6.60	27.96
60	570.94	766.16	788.72	6.65	27.25
86	568.00	765.18	769.10	6.62	28.0
100	561.13	757.33	793.63	6.74	26.95
150	567.02	753.41	783.82	6.75	27.05
172	570.94	760.28	784.80	6.44	28.05

TABLE 6.2

The Central Composite Statistical Design for the Investigation.

Variable			Levels				
			-2	-1	0	+1	+2
i	Slide angle	(θ,degrees)	10	15	20	25	30
ii	Nose angle	(2γ, degrees)	62.5	75	86.5	100	112.5
iii	Lift height	(H, cm)	1.66	2.30	2.94	3.58	4.22
iv	Soil depth	(D, cm)	1.27	2.54	3.81	5.08	6.35
v	Speed	(V, cm/sec.)	83.0	97.0	111.0	125.0	139.0

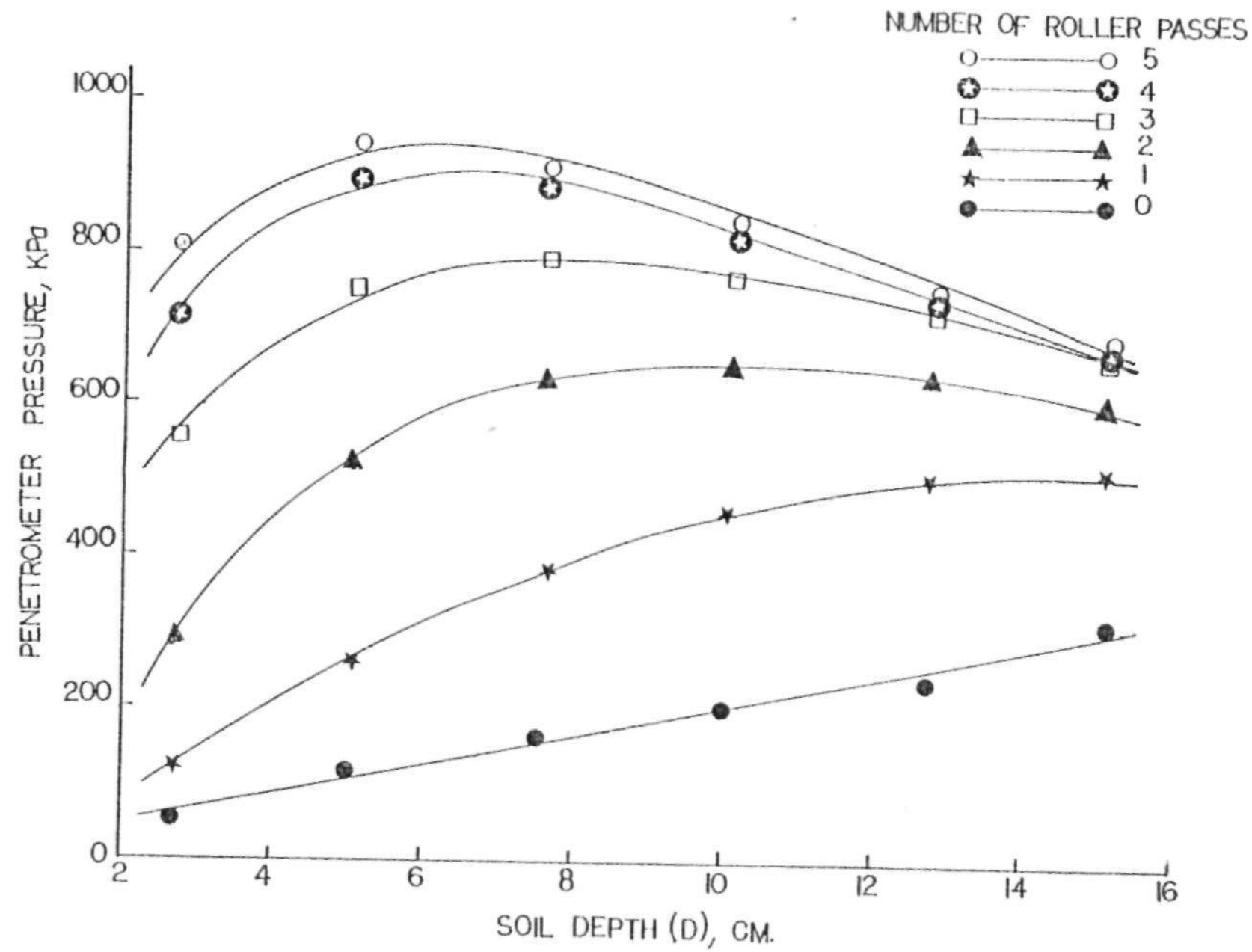

Fig. 6.2 Penetrometer Pressure Variation with Depth in the Soil Bin

shearing resistance, and the coefficient of soil-metal friction are important parameters of the model equations. The methods adopted for investigating these properties are the direct shear test and the insitu test with the Cohron shear graph.

For the direct shear test, the amount of soil sample used was determined from the known soil density and the volume of the direct shear apparatus, excluding the heights of the top and bottom porous plates. The shear machine was calibrated for normal pressures of 96kPa, 192kPa, 288kPa, 384kPa and 480kPa respectively. The corresponding gage pressures were 24kPa, 48kPa, 72kPa, 96kPa and 120 kPa respectively. The prepared sample was fixed in place in the shear unit and the vertical and horizontal dial gages positioned on the machine. The vertical dial gage measured the vertical displacement while the horizontal dial gage measured the horizontal displacement. The shear force corresponding to each normal force was recorded on a chart recorder which continuously plotted the shear force as the test progressed. The shear stress for each test was computed and the peak stress obtained was used for plotting the shear stress normal stress graph as shown in Fig. 6.3. The maximum obtainable strain rate for this machine without excessive vibration was 0.90 mm per minute. Even though this may be low compared to the rate at which a soil is strained during the passage of any tool, the result obtained is not at great variance from that obtained using the Cohron shear graph.

The Cohron shear graph was placed on the surface of the prepared soil and its metal head (cup) introduced into the soil vertically at slow rate. This metal head is equipped with internal vanes to ensure soil-soil shearing action. The shear tests were conducted along the test path at four locations and the results averaged.

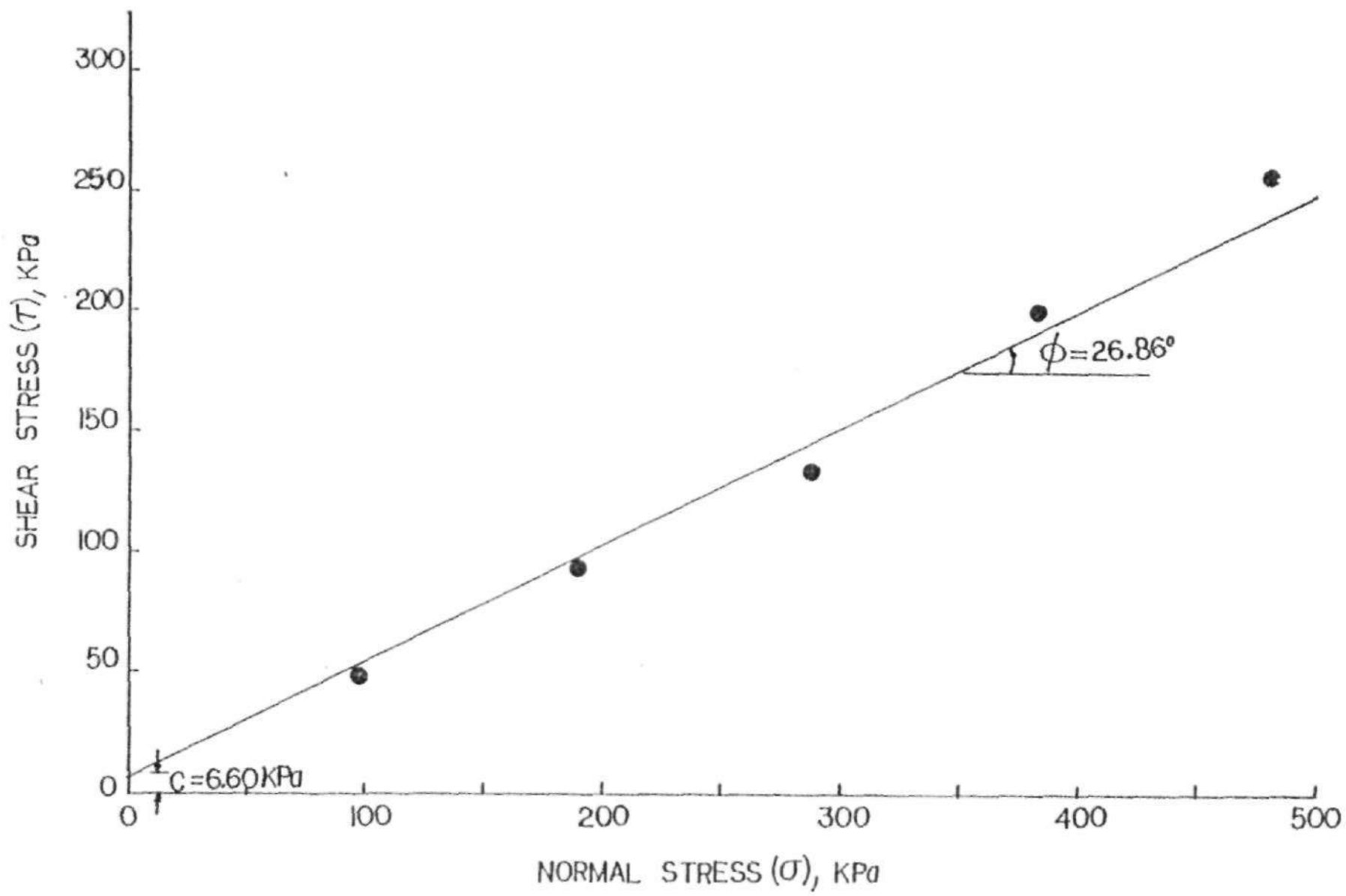

Fig. 6.3 Shear Stress vs Normal Stress Curve for Direct Shear Test on Artificial Soil

The angle of soil-metal friction was also measured directly on the surface of the prepared soil. A metal slider with a surface area of 232 sq. cm was prepared from the 3.2 mm thick cold-rolled steel, the same material used for fabricating the model tools. This plate was loaded with varying known weights and pulled along the soil surface with a calibrated spring type dynamometer. The value of the tangential force corresponding to each normal force was used in computing the tangential stress versus normal stress from which the soil-metal frictional angle and hence the coefficient of soil-metal friction were obtained. The assumption made in the mathematical model that the force of adhesion is negligibly small was confirmed in this test as shown in Fig. 6.4.

The strength distribution in the soil profile was further checked using a hand held cone penetrometer. A 30° cone penetrometer with a 3.20 cm base area was used for the test. With the cone tip placed on the soil and the stem held vertically, the tip was introduced into the soil at a slow rate. Observations were made for cone depths of 0 to 15 cm in 2.54 cm increments, and the results of average penetrometer pressure versus soil depth was plotted as shown in Fig. 6.2. The soil strength consistency was periodically checked with this equipment throughout the conduct of the experiment as presented in Table 6.1.

6.3 Experimental Design:

The primary objective of this study was to investigate how the geometric designs of undercutters, operational speeds and the soil operating depths influence draft performance. A central composite statistical design was found to be best suited for this study. Five levels of tool lift height, nose angle, slide angle, soil depth and operational speed were selected as shown in Table 6.2. The width of 38.1cm was used for this study. The range of soil depths and tool speeds were scaled in

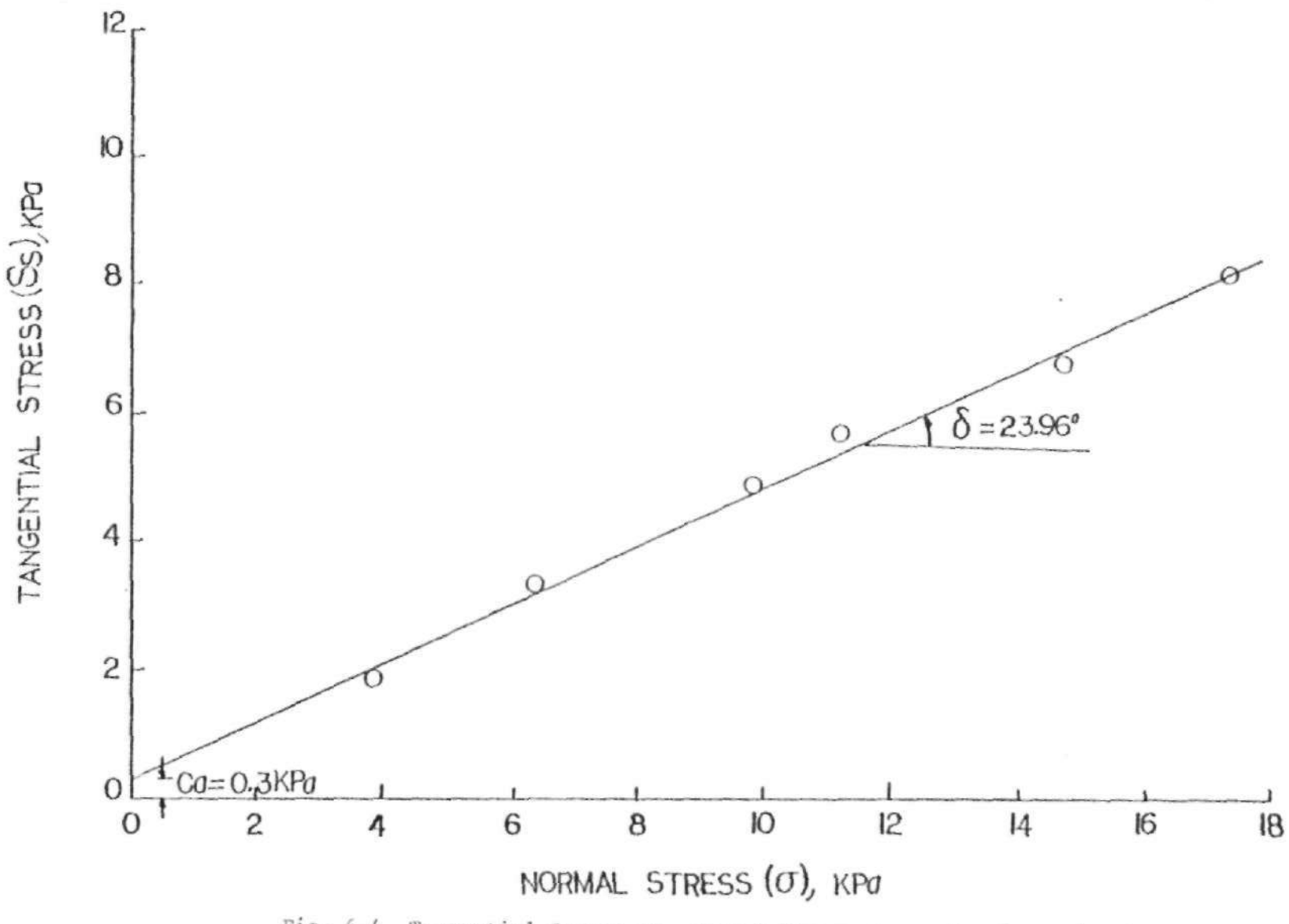

Fig. 6.4 Tangential Stress vs. Normal Stress Curve for Determination of Soil-metal Interface Properties in the Soil Bin

accordance with the scale of model to prototype (true size) used. The speeds were selected by calibrating the flow rate of the hydraulic motor which drives the carriages. The calibration curve is shown in Fig. 6.5. A total of twenty-nine model tools were constructed for this study as shown in Table 6.3 and in Figures 6.6(a)and 6.6(b)respectively.

6.4 Data Acquisition and Reduction:

A SYM-1 microcomputer, manufactured by Synertek Systems Corporation, was used in conjunction with the multichannel recorder for the data acquisition as shown in Fig. 6.7. Each load cell was calibrated prior to its installation by hanging known weights on it and monitoring the corresponding force response with the microcomputer via the recorder. Since there are six load cells, only six channels on the recorder were utilized. The appropriate gain and balance were selected on the recorder and the calibration constant read from the digital display on the microcomputer. The span on the recorder was adjusted to give a voltage reading of 5v to 10v. The zero balance was rechecked after removing the dead weights and the process repeated until consistent values were obtained. The calibration constants were checked periodically during the conduct of the experiment. This single board, 28 key microcomputer was programmed to sample 20 data points per second for five seconds. The test length of the bin is 5 meters. One test run was made for each soil preparation. Prior to each test run, a hole was dug and the model tool lowered to the prescribed depth. The flow rate of the hydraulic motor was then selected and the calibration constants on the microcomputer checked. Data generated from each test run was stored on a cassette tape. This information is in hexadecimal form. It was later transferred into the departmental Digital Equipment Corporation minicomputer via the

TABLE 6.3

Geometric Elements Used for Designing Model Tools

Tool No.	Lift Height H	Slide Angle θ	Nose Angle γ	Tool Width W	Incline Angle β	Bevel Angle α	Wing Width w	Slide Length S	Wing Major Length L1	Minor Length L2	Surface Wing Aw	Area Total At
1	2.30	15.00	37.50	38.10	23.76	39.98	5.71	8.89	31.29	24.48	159.22	318.44
2	2.30	15.00	50.00	38.10	19.28	51.62	6.97	8.89	24.87	19.35	154.02	308.03
3	2.30	25.00	37.50	38.10	37.45	44.03	3.78	5.44	31.29	27.38	110.96	221.92
4	3.58	15.00	37.50	38.10	23.76	39.98	8.89	13.83	31.29	20.69	230.99	461.98
5	2.30	25.00	50.00	38.10	31.33	54.37	4.42	5.44	24.87	21.70	102.99	205.98
6	3.58	15.00	50.00	38.10	19.28	51.62	10.84	13.83	24.87	16.28	223.08	446.17
7	3.58	25.00	37.50	38.10	37.45	44.03	5.89	8.47	31.29	25.20	166.30	332.60
8	3.58	25.00	50.00	38.10	31.22	54.37	6.89	8.47	24.87	19.93	154.23	308.46
9	3.58	20.00	43.75	38.10	27.76	47.25	7.69	10.47	27.55	20.44	184.44	368.88
10	2.30	20.00	43.75	38.10	27.76	47.25	4.94	6.72	27.55	22.98	124.77	249.53
11	2.94	25.00	43.75	38.10	33.99	49.10	5.26	6.96	27.55	22.99	132.89	265.78
12	2.94	15.00	43.75	38.10	21.18	45.75	8.14	11.36	27.55	19.62	191.92	383.83
13	2.94	20.00	50.00	38.10	25.41	52.84	6.85	8.60	24.87	19.68	152.58	305.16
14	2.94	20.00	37.50	38.10	30.87	41.80	5.73	8.60	31.29	24.88	160.93	321.85
15	2.94	20.00	43.75	38.10	27.76	47.25	6.31	8.60	27.55	21.71	155.40	310.95
16	1.66	10.00	31.25	38.10	18.77	32.66	5.16	9.56	36.72	28.67	168.66	337.32
17	1.66	10.00	56.25	38.10	11.97	56.83	8.00	9.56	22.91	17.68	162.41	324.81
18	1.66	30.00	31.25	38.10	48.06	42.24	2.23	3.32	36.72	34.26	79.21	158.41
19	4.22	10.00	31.25	38.10	18.77	32.66	13.11	24.30	36.72	16.26	347.38	694.77
20	1.66	30.00	56.25	38.10	34.78	61.24	2.91	3.32	22.91	21.31	64.36	128.72
21	4.22	10.00	56.25	38.10	11.97	56.83	20.34	24.30	22.91	9.61	330.82	661.64
22	4.22	30.00	31.25	38.10	48.06	42.24	5.67	8.44	36.72	30.47	190.61	381.21
23	4.22	30.00	56.25	38.10	34.78	61.24	7.40	8.44	22.91	18.85	154.49	308.99
24	4.22	20.00	43.75	38.10	27.76	47.25	9.06	12.34	27.55	19.17	211.66	423.31
25	1.66	20.00	43.75	38.10	27.76	47.25	3.56	4.85	27.55	24.25	92.31	184.62
26	2.94	30.00	43.75	38.10	39.86	51.27	4.59	5.88	27.55	23.87	117.94	235.87
27	2.94	10.00	43.75	38.10	14.30	44.65	11.90	16.93	27.55	15.50	256.14	512.27
28	2.94	20.00	31.25	38.10	35.05	36.55	5.12	8.60	36.72	29.82	170.30	340.60
29	2.94	20.00	56.25	38.10	23.64	58.53	7.33	8.60	22.91	18.42	151.52	303.05

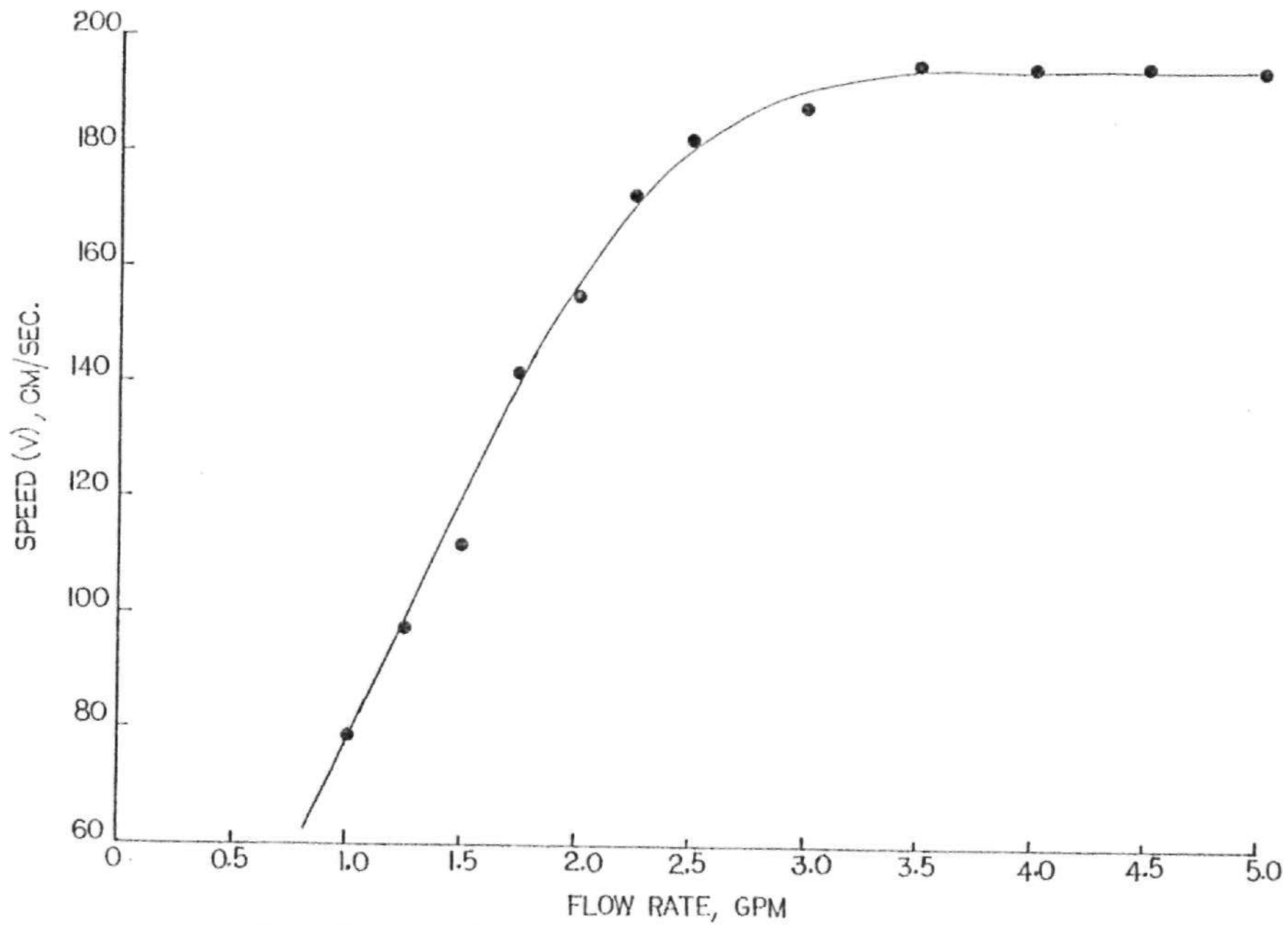

Fig. 6.5 Calibration Curve for the Hydraulic Motor Pump on the Soil Bin

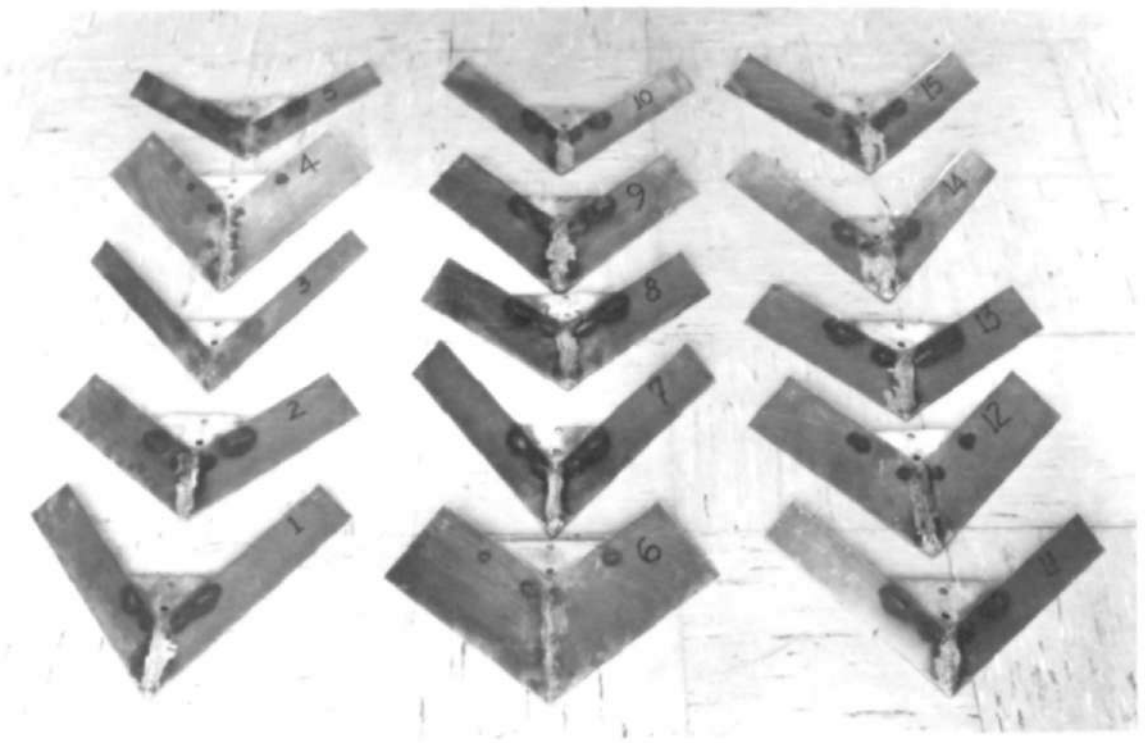

(a)

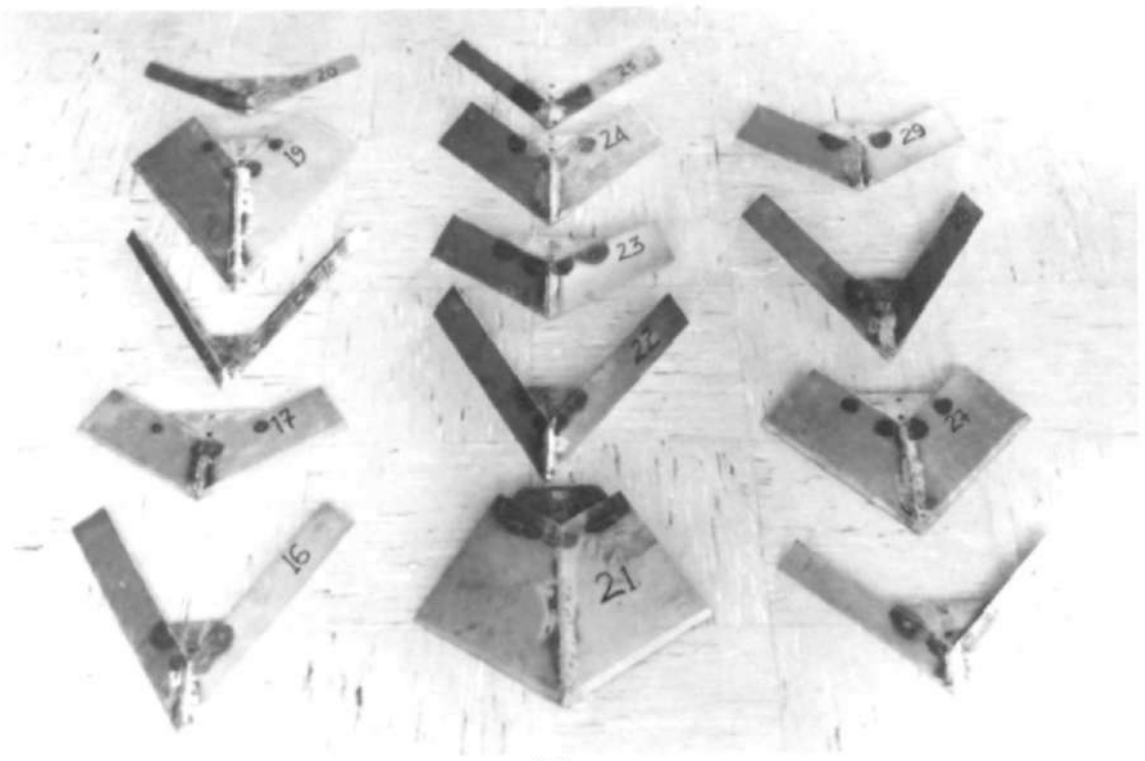

(b)

Fig. 6.6 Twenty-nine Model Tools Designed for this Investigation

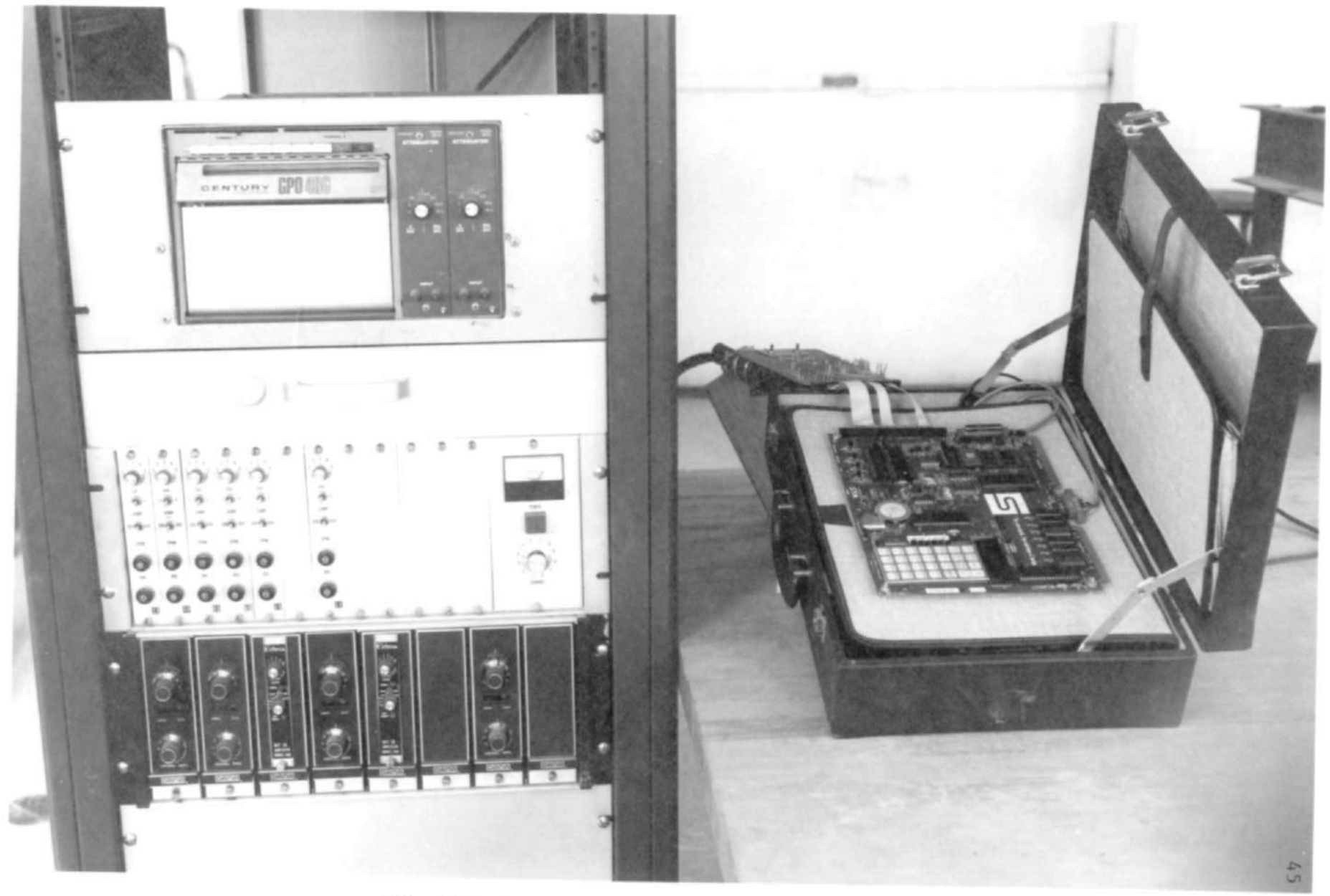

Fig. 6.7 Laboratory Data Acquisition System

CRT terminal. Data reductions were performed once data were put on the minicomputer. The schematics of the data aquisition system is shown in Fig. 6.8.

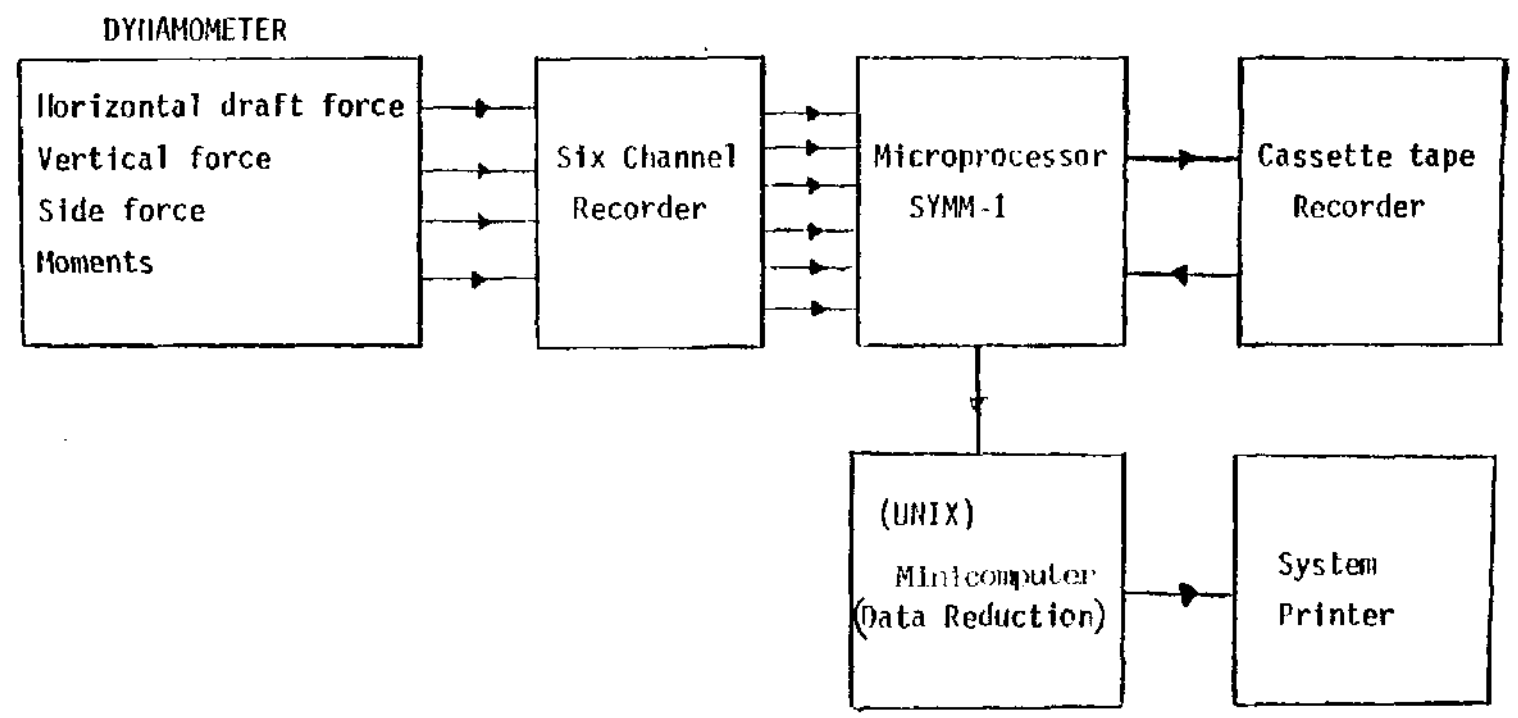

Fig. 6.8 Schematics of Data Acquisition System

Chapter VII

RESULTS AND DISCUSSIONS

The objectives of this dissertation included:

1. Experimental study of the various tool and soil parameters that influence the design and application of undercutters based on their draft power requirement.
2. The verification of an analytical model to predict draft force on this tool type.

7.1 Experimental Study

Prior to the conduct of this experiment, a consistent method of processing the soil was established. Soil density tests were performed to determine variation of soil density with soil depth. Three roller passes provided the least variation with depth. However, greater soil compaction existed at the surface of the prepared soil and an attempt to completely eliminate this was unsuccessful. A direct shear test and cohron shear graph test were employed for the determination of pertinent soil strength parameters.

The average soil density value, obtained for three roller passes, was 15.50kN/m^3. This soil density value was used for the determination of soil strength properties using the direct shear apparatus. The resulting values of soil cohesion and the angle of soil shearing resistance were 6.60kPa and 26.86 degrees respectively. The angle of soil-metal friction was determined on the surface of the prepared soil. Its value was 24 degrees.

Each of the twenty-nine model tools discussed in Chapters V and VI were experimentally tested based on the statistical design for this

investigation. The observed soil failure pattern depended, to a large extent, on the depth of operation and the tool geometry and apparently was influenced little by the range of velocities used. The surface of the soil after running tool No. 15 at 1.27 cm deep and 3.81 cm deep respectively are shown in Figures 7.1 and 7.2. The velocity of operation in both cases was 97 cm/sec. A contrasting appearance of the soil surface was also observed between tool No. 21 and tool No. 22. At shallow depth (1.27 cm) there was little typical soil cutting with tool No. 21 as the tool essentially bulldozed the soil. A smooth even surface was observed for tool No. 22 at this depth. However at greater depth (6.35 cm) a fairly even surface was observed for tool No. 21. while a trough was left in the middle of the worked surface by tool No. 22. It is not exactly clear which of the soil and tool factors were responsible for these conditions but the effects were quite noticeable. The bulldozing effect at shallow depth by some of these tools accounted for the unreasonably high draft forces observed for some of these model tools. A close study of Table 6.3 and Appendix C.7.1 will reveal variations in observed results for the geometric design of each tool. The bulldozing effect of tool No. 21 is shown in Fig. 7.3.

7.2 Analytical Study

The mechanics of equilibrium and vector algebra were employed in establishing the mathematical model equation used to predict draft forces on the model tools. By comparing the resulting draft forces shown in Appendix C (C.7.4 and C.7.5), it can be seen that predicted draft result is, in most cases, lower than observed forces, and the difference is more extreme for some of the model tools at shallow depths. This is possibly due to the observed variations in soil density with depth and the fact that the model results were not subjected to extraneous

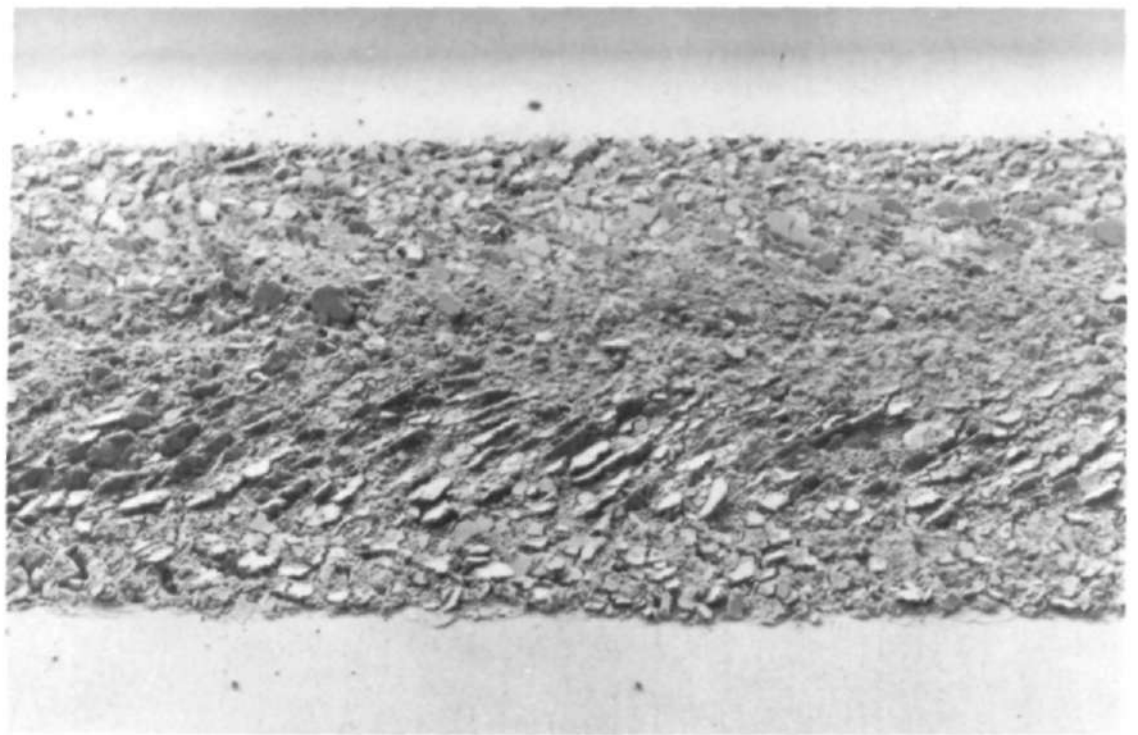

Fig. 7.1 Soil Surface Profile for Model Tool No. 15
Operated at a Soil Depth of 1.27 cm (V = 97 cm/sec.)

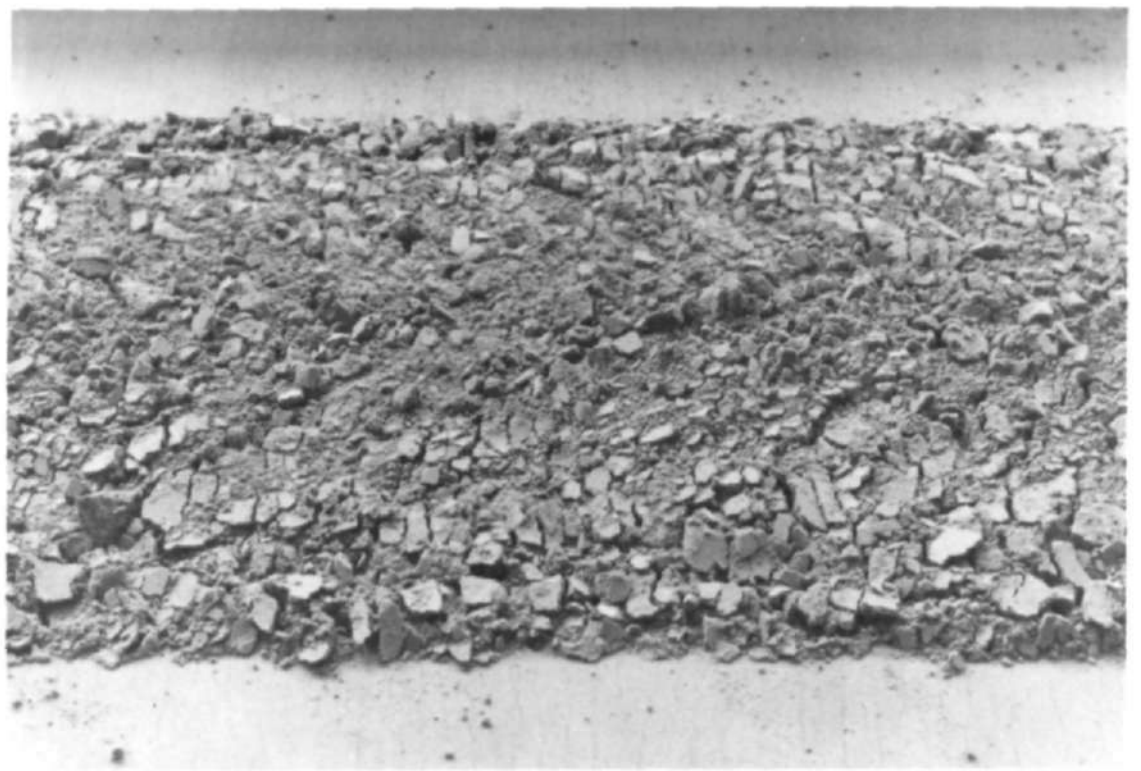

Fig. 7.2 Soil Surface Profile for Model Tool No. 15
Operated at a Soil Depth of 3.81 cm (V = 97 cm/sec.)

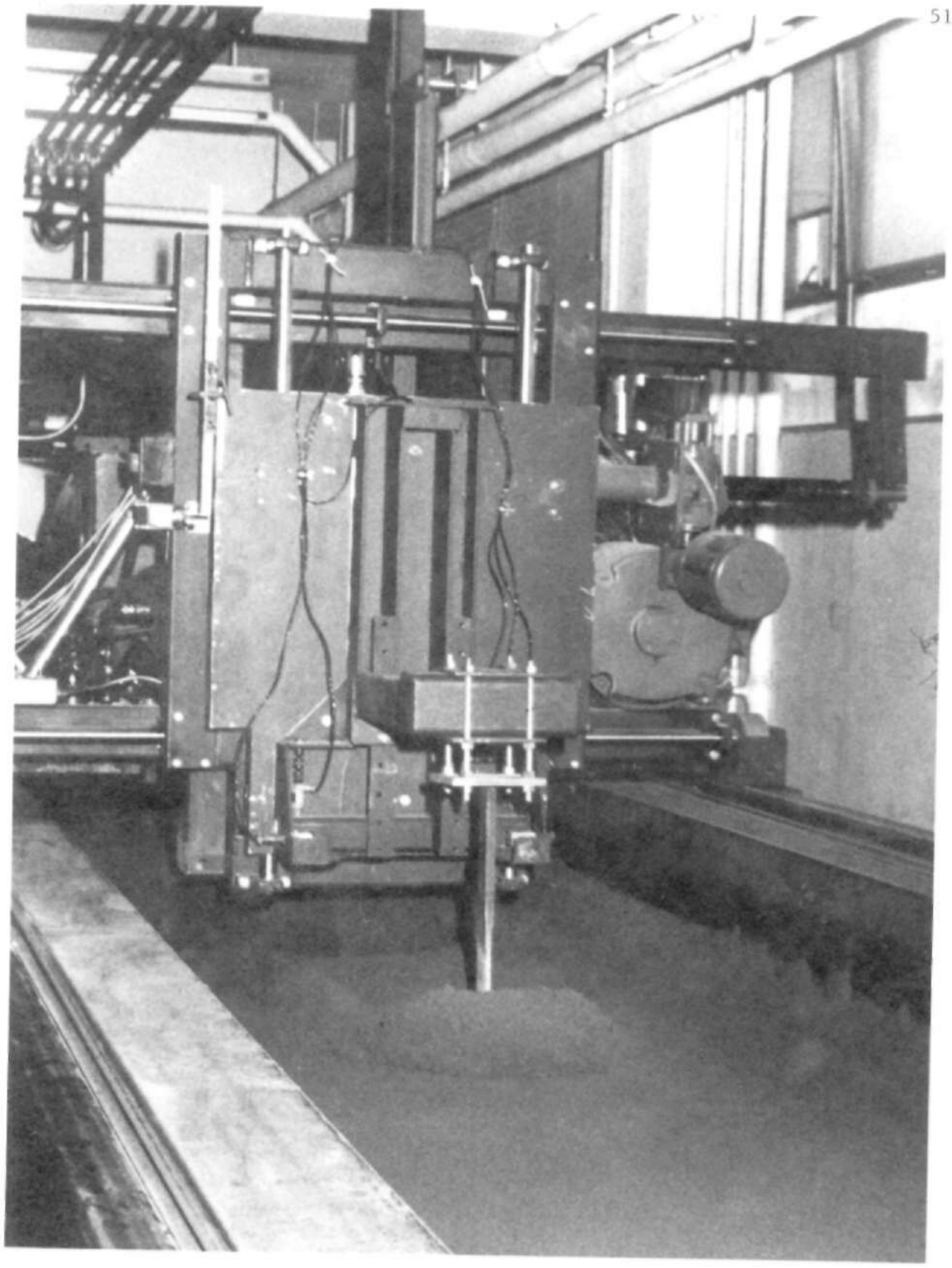

Fig. 7.3 Bulldozing Effect of Tool No. 21 at a Shallow Depth
(D = 1.27 cm V = 83 cm/sec.)

factors to which the experimental model tools were subjected. Since soil shearing resistance is influenced by soil density and soil depth is shown to influence soil density, it is highly probable that soil shearing resistance changed with soil depth. This was assumed to be constant in the mathematical model. The difficulty in modeling soil stress conditions can be advanced to explain the differences in the experimental and theoretical results.

7.3 Statistical Analysis of the Data

The statistical design of this investigation is to provide information on the influence of each of the factors on draft. These factors are soil depth (D), tool velocity (v), tool slide angle (θ), tool lift height (H) and the tool nose angle of the tool (2γ). The central composite design adopted enabled one to study the variations in draft with levels of one factor at selected levels of the other factors. The preliminary statistical analysis of the data using general linear model building techniques showed that the draft force varies exponentially with the factors as revealed by the parabolic form of the preliminary graphs. This suggests that no single factor can be investigated in the absence of other factors.

A model building technique that would include all the first second and third order terms and their interactions was thought best for analyzing these data. This was done through the use of the statistical packages (SAS79) that are available at KSU Computing Center.

A backward elimination procedure was employed for each set of data. The results of these analyses are presented in Tables 7.1 and 7.2. Data shown in Appendix C.7.1 were used in this analysis and a statistical model was developed from the draft (experimental) and

Table 7.1. Backward Elimination Procedure For Experimental Model-Draft

R^2 =0.96774 C(P)=7.05154

	DF	SUM OF SQUARES	MEAN SQUARE	F	PROB>F
REGRESSION	15	1582969.63911	105531.309274	311.96	0.0001
ERROR	156	52772.61526	338.285995		
TOTAL	171	1635742.25437			

	B VALUE	STD. ERROR	TYPE II SS	F	PROB>F
INTERCEPT	82.94588				
D	21.622142	4.872609	6661.287914	19.69	0.0001
HΘ	-1.523795	0.173265	26164.708047	77.34	0.0001
HY	2.018007	0.589905	3958.822879	11.70	0.0008
DΘ	0.364065	0.087685	5831.652206	17.24	0.0001
DY	-0.226995	0.702430	3532.730488	10.44	0.0015
ΘY	0.269411	0.037031	17904.856956	52.93	0.0001
V^2	0.001018	0.000568	1086.309831	3.21	0.0751
Y^2	-0.262142	0.060524	6346.077436	18.76	0.0001
H^2	0.934627	0.374823	2103.340833	6.22	0.0137
Y^3	0.003527	0.000805	6490.461715	19.19	0.0001
HD^2	2.554007	0.315162	22215.778963	65.67	0.0001
H^2D	-2.646502	0.420004	13431.408620	39.70	0.0001
H^2V	0.018832	0.010476	1093.340997	3.23	0.0741
$ΘY^2$	-0.003826	0.000558	15886.743735	46.96	0.0001
HY^2	0.266329	0.106717	2106.936437	6.23	0.0136

Table 7.2. Backward Elimination Procedure For Analytical Model-Pdraft

$R^2 = 0.99966$ C(P)=15.80250

	DF	SUM OF SQUARES	MEAN SQUARE	F	PROB>F
REGRESSION	21	1516344.885533	72206.899311	21107.46	0.0001
ERROR	150	513.137719	3.420918995		
TOTAL	171	1516858.023252			

	B VALUE	STD. ERROR	TYPE II SS	F	PROB>F
INTERCEPT	59.384452				
H	95.969535	5.167248	1180.024095	344.94	0.0001
D	73.057588	1.137782	14079.753740	4115.78	0.0001
γ	-9.226946	2.236396	58.242341	17.03	0.0001
HD	-21.691233	0.849060	2232.722602	652.67	0.0001
HV	-0.077977	0.027066	28.393085	8.30	0.0045
Hθ	-0.184857	0.017489	382.214050	111.73	0.0001
DV	0.045543	0.003131	724.047351	211.65	0.0001
Dθ	0.986968	0.008823	42806.431655	12513.14	0.0001
Dγ	-0.647564	0.007064	28744.977122	8402.71	0.0001
Vθ	0.009918	0.000786	544.659396	159.21	0.0001
Vγ	-0.002419	0.000615	52.994927	15.49	0.0001
$\theta\gamma$	-0.314296	0.052661	121.856795	35.62	0.0001
H^2	-15.404114	0.888021	1029.365516	300.90	0.0001
θ^2	0.218767	0.058385	48.029697	14.04	0.0003
γ^3	0.212634	0.046796	70.628636	20.65	0.0001
θ^3	-0.002201	0.000991	16.878145	4.93	0.0278
γ^3	-0.001500	0.000342	65.635814	19.19	0.0001
HD^2	0.205670	0.035177	116.943440	34.18	0.0001
H^2D	3.713766	0.136510	2531.875191	740.12	0.0001
H^2V	0.013299	0.004958	24.616250	7.20	0.0081
$\theta\gamma^2$	0.003474	0.000602	114.054433	33.34	0.0001

predicted draft data respectively. For the experimental data, the resulting model is:

$$\text{Experimental Model, Draft} = 82.946+21.622D-1.524H\theta+2.018H\gamma+0.364D\theta -0.227D\gamma+0.269\theta\gamma+0.001V^2-0.262\gamma^2+0.935H^3 +0.004\gamma^3+2.554HD^2-2.647H^2D+0.019H^2V -0.004\theta\gamma^2-0.266H^2\gamma$$

The R^2 value is 0.96774. This value represents the percentage of total data variation that is explained by the model. Depth is the only single factor in the model which further explains the dorminant role of tillage depth in this investigation. The error mean square for this model is 388.3 and is an indication of the magnitude of extraneous or environmental factors.

The resulting statistically developed model for the predicted (analytical) draft (Pdraft) data is as follows:

$$\text{Analytical Model, Pdraft} = 59.384+95.970H+73.058D-9.227\gamma-21.691HD -0.078HV-0.185H\theta+0.0455DV+0.987D\theta-0.648D\gamma +0.010V\theta-0.002V\gamma-0.314\theta\gamma-15.404H^2+0.219\theta^2 +0.213\gamma^2-0.002\theta^3-0.002\gamma^3+0.206HD^2+3.714H^2D +0.0133H^2V+0.004\theta\gamma^2$$

The R^2 value is 0.99966. This means there is less variation in the total data as explained by the model. This is expected because these data were not collected under the same environment as for the experimental data. The error mean square of 3.4209 confirmed this belief. It should, however, be observed that there are more single factors in the analytical model (Pdraft) equation than in the experimental model Draft equation. This does not make the latter less accurate because these single factors may be significantly present in the interactions.

7.4 Discussion of the Results

The statistically developed model equations were used to generate data presented in Tables 7.3 and 7.4 and those in the Appendix C.7.4 to C.7.5. Data in Tables 7.3 and 7.4 were used in plotting the graphs shown in Figures 7.4 and 7.5 respectively. The main advantage to this is that the equations provide a smoothing of the curves thereby making their interpretations easier. The Figures were for experimental model (Draft) and the analytical model (Pdraft) which represent the observed analytical results respectively.

7.4.1 Influence of Soil Depth on Draft

Figure 7.4 shows the influence of depth of operation on draft for model Draft and model Pdraft respectively. In both cases, increasing the depth of tool operation brings about an increase in draft for given levels of tool lift height, slide angle and nose angle. The range of velocity used to generate the data was 75 cm/sec. to 135 cm/sec. The relationship of depth with draft is parabolic and is represented by the upward shifts in the graphs. The contribution of soil depth to the overall draft is obvious from this figure and from the tables in the Appendix C.7.4 to C.7.5. The draft increase with depth is due to the increase in the weight of soil segment passing over the surface of the tool. This increase in the weight of soil segment results in an increase in the force needed to accelerate and lift the soil segment. Undercutters are usually operated at shallow depths (6-10 cm) aimed at causing minimum disturbance to the wind erosion-prone soils. The importance of depth to these models is further reflected in Tables 7.1 and 7.2 where direct and interactive effects are shown. Depth is, infact, the most dominant single factor in the models.

Table 7.3. Experimental Model(Draft) and Analytical Model(Pdraft) Data
For Different Soil Depths

				DRAFT					PDRAFT				
				SOIL DEPTH(CM)					SOIL DEPTH(CM)				
H	θ	2Y	V	2	3	4	5	6	2	3	4	5	6
2	15	75	75	92.12	125.64	169.38	223.33	287.50	72.11	112.63	153.96	196.14	239.12
			90	95.77	129.30	173.03	226.99	291.16	72.81	114.01	156.04	198.88	242.55
			105	99.89	133.41	177.15	231.10	295.27	73.51	115.39	158.10	201.63	245.98
			120	104.46	137.98	181.72	235.67	299.84	74.21	116.78	160.17	204.38	249.42
			135	109.49	143.01	186.95	240.70	304.86	74.91	118.16	162.23	207.13	252.85
2	25	75	75	115.94	153.10	200.48	258.07	325.88	87.50	137.89	189.10	241.14	294.00
			90	119.59	156.75	204.13	261.72	329.53	89.69	140.76	192.65	245.37	298.91
			105	123.70	160.86	208.24	265.83	333.64	91.87	143.63	196.20	249.60	303.83
			120	128.27	165.43	212.81	270.40	338.21	94.06	146.50	199.75	253.84	308.74
			135	133.30	170.46	217.84	275.43	343.24	96.24	149.36	203.31	258.07	313.66
3	15	100	75	99.74	129.96	175.51	236.37	312.56	70.85	101.18	132.74	165.54	199.58
			90	104.81	135.03	180.57	241.44	317.63	70.92	101.94	134.19	167.67	202.38
			105	110.33	140.55	186.09	246.96	323.15	71.00	102.70	135.63	169.79	205.19
			120	116.31	146.53	192.07	253.94	329.13	71.08	103.46	137.01	171.92	208.00
			135	122.75	152.97	198.51	259.38	335.57	71.16	104.22	138.51	174.04	210.81
3	25	100	75	100.05	133.91	183.10	247.60	327.43	83.38	123.59	165.02	207.69	251.59
			90	105.12	138.98	188.16	252.67	332.50	84.95	125.83	167.95	211.30	255.89
			105	110.64	144.50	193.68	258.19	338.12	86.51	128.08	170.88	214.91	260.18
			120	116.62	150.48	199.66	264.17	344.00	88.07	130.32	173.80	218.52	264.47
			135	123.06	156.92	206.10	270.61	350.44	89.64	132.57	176.73	222.13	268.77

Table 7.3. Experimental Model(Draft) and Analytical Model(Pdraft) Data For Different Soil Depths (cont.)

				DRAFT					PDRAFT				
				SOIL DEPTH(CM)					SOIL DEPTH(CM)				
H	θ	2Y	V	2	3	4	5	6	2	3	4	5	6
4	30	110	75	85.13	113.91	163.13	232.78	322.86	91.69	138.93	187.80	238.33	294.50
			90	92.16	120.95	170.16	239.81	329.89	94.05	141.96	191.52	242.73	295.58
			105	99.66	128.44	177.66	247.31	337.39	96.40	145.00	195.24	247.13	300.66
			120	107.61	136.40	185.61	255.26	345.34	98.75	148.03	198.96	251.53	305.74
			135	116.03	144.81	194.03	263.68	354.76	101.10	151.06	202.67	255.93	310.82

TABLE 7.4. Experimental Model(Draft) and Analytical Model(Pdraft) Data
For Different Tool Slide Angles

				DRAFT					PDRAFT				
				SLIDE ANGLE, θ (DEGREES)					SLIDE ANGLE, θ (DEGREES)				
D	H	2Y	V	10	15	20	25	30	10	15	20	25	30
3	2	60	75	135.75	149.09	162.42	175.76	189.09	130.10	137.50	150.89	168.62	189.04
			90	139.40	152.74	166.07	179.41	192.74	131.02	139.16	153.29	171.78	192.92
			105	143.52	156.86	170.19	183.52	196.86	131.93	140.81	159.68	174.90	196.80
			120	148.09	161.42	174.76	188.09	201.43	132.84	142.46	158.08	178.03	200.68
			135	152.12	153.12	179.79	193.12	206.46	133.75	144.12	160.47	181.17	204.56
3	2	75	75	111.92	125.64	139.37	153.10	166.83	108.16	112.63	123.09	137.89	155.38
			90	115.57	129.30	143.02	156.75	170.48	108.80	114.01	125.21	140.76	158.99
			105	119.68	133.41	147.14	160.86	174.59	109.44	115.39	127.34	143.63	162.60
			120	124.25	137.98	151.71	165.43	179.16	110.08	116.79	129.47	146.49	166.21
			135	129.28	143.01	156.74	170.46	184.19	110.72	118.16	131.59	149.36	169.82
3	2	100	75	100.81	110.40	120.00	129.59	139.19	89.41	93.38	103.34	117.64	134.62
			90	104.46	114.06	123.65	133.25	142.84	89.60	94.31	105.01	120.05	137.79
			105	108.57	187.17	127.76	137.36	146.95	89.79	95.25	106.69	122.47	140.95
			120	113.14	122.74	132.33	141.93	151.52	89.98	96.18	108.36	124.89	144.11
			135	118.17	127.77	137.36	146.96	156.55	90.17	97.11	110.04	127.31	147.27